THEORETICAL EVALUATION OF ENGINE AUXILIARY INLET DESIGN FOR SUPERSONIC V/STOL AIRCRAFT

Michael A. Boles

and

Richard L. Heavner

Prepared for

NASA - Lewis Research Center
Under Grant Number NAG 3-608

August 1988

Department of Mechanical and Aerospace Engineering
North Carolina State University
Raleigh, North Carolina 27695-7910

ABSTRACT

A higher order panel method is used to evaluate the potential flow of a 2-D supersonic V/STOL inlet. A non-symmetric analytical inlet model is developed to closely match a wind tunnel model tested at NASA Lewis Research Center. The analytical inlet used in this investigation is analyzed for flow characteristics around the lower cowl lip and auxiliary inlets. The results for this analysis are obtained from the output of a computer program produced by the McDonnell Douglas Corporation. This program is based on the Hess Panel Method which determines source strengths of panels distributed over a three-dimensional body.

The analytical model was designed for the implementation of a drooped/translated cowl lip and auxiliary inlets as flow improvement concepts. A 40 or 70 degree droop lip can be incorporated on the inlet to determine if these geometry modifications result in flow improvements which may reduce the propensity for flow separation on the interior portion of the lip. Auxiliary inlets are employed to decrease the mass flow over the inlet lip; thus, the peak flow velocity is reduced at the lip which also lessens the likelihood of flow separation on the interior portion of the lip. A 2, 4, and 6 in. (5.08, 10.16, and 15.24 cm) translated lip can be employed to also decrease mass flow over the inlet lower lip in the same manner as the auxiliary inlet.

The performance results of the flow improvement concepts show that three possible inlet configurations provide a situation where separation is less likely to occur. A 70 degree droop lip maintains flow conditions such that attached flow over the lower cowl lip may exist for the entire angle of attack range studied. A 0 degree droop and translated lip combination provides similar results for the angle of attack range. The third configuration consists of a 0 degree droop and auxiliary inlet combination. This configuration provides slightly less favorable results than the other two, but still allows for conditions favorable to attached flow within the inlet.

TABLE OF CONTENTS

LIST OF FIGURES

LIST OF FIGURES (Continued)

Page

LIST OF FIGURES (Continued)

Page

LIST OF FIGURES (Continued)

Page

LIST OF FIGURES (Continued)

Page

LIST OF SYMBOLS

A_i	left side integral coefficient or inlet cross-sectional area
A_{th}	throat cross-sectional area
b_i	boundary condition value
D	inlet interior hydraulic diameter
CR	contraction ratio A_i/A_{th}
H	total exterior height of inlet
H_1	height of supersonic V/STOL inlet from upper cowl lip highlight to upper exterior surface
H_2	height of supersonic V/STOL inlet from center of coordinate system to upper exterior surface
H_3	height of supersonic V/STOL inlet from center of coordinate system to lower cowl lip highlight
h	inlet thickness
L	inlet length
L_1	length of exterior upper surface ramp of the supersonic V/STOL inlet
L_2	length of interior upper surface ramp of the supersonic V/STOL inlet
L_3	length from center of coordinate system to the lower cowl lip highlight on the supersonic V/STOL inlet
n	unit normal vector
P	general point where potential and velocity are evaluated
P′	point on the body surface where potential and velocity are evaluated
P_s	surface static pressure
P_t	total pressure
p	fluid pressure
q	source point on the body surface

LIST OF SYMBOLS (Continued)

R'	region exterior to body surface
r	distance from a point where potential and velocity are evaluated to a source point
R_1/t	forward ramp auxiliary inlet radius ratio
R_2/t	aft-ramp auxiliary inlet radius ratio
S	body surface for which flow is computed
t	auxiliary inlet thickness
V	total velocity vector
$\bar{V}_\infty$	onset velocity vector or freestream velocity
V_c	local compressible velocity
V_i	local incompressible velocity
$\bar{V}_i$	average incompressible velocity across the flow area
v	disturbance velocity vector due to the body surface
x	x-coordinate of the global coordinate system
x_{hl}	x-coordinate of the highlight location
x_q	x-coordinate of the point q
y	y-coordinate of the global coordinate system
y_q	y-coordinate of the point q
z	z-coordinate of the global coordinate system
z_q	z-coordinate of the point q
α	angle of attack
δ	slot distance
ρ	fluid density
$\bar{\rho}_c$	average compressible density across the flow area
ρ_i	incompressible density

LIST OF SYMBOLS (Continued)

σ	surface source density
ϕ	velocity potential

INTRODUCTION

Recently there has been increasing investigation of the flow characteristics of a high performance supersonic engine inlet at low flight Mach numbers. The engine inlet on the vertical/short takeoff and landing (V/STOL)aircraft has been the focal point of this analysis. The purpose of this investigation is to determine the best geometrical configuration of a complicated three-dimensional supersonic model inlet during vertical/short takeoff and landing maneuvers at low speeds.

Figure 1 shows a typical supersonic V/STOL aircraft configuration which employs a 2-D supersonic V/STOL engine inlet. Low speed wind tunnel analysis of the engine inlet has been completed at the NASA Lewis Research Center (Ref. 1). An analytical non-symmetric three-dimensional inlet model which closely matches the specifications of the NASA 2-D inlet is developed in this report. This inlet model is flexible in that numerous inlet configurations, which include various cowl lip geometries and auxiliary inlets may be evaluated at specified angles of attack, freestream Mach numbers, and fan face Mach numbers. The results produced will provide information to developers of V/STOL supersonic inlets for further design modifications.

A V/STOL engine inlet experiences high angle of attack flow during the transition from thrust supported operation to wing borne flight. For example, high angle of attack flow may result from ingested flow when the aircraft is near ground contact. As the flow proceeds downstream into the inlet, the resulting decrease in surface static pressure can lead to large regions of flow separation resulting in

loss of thrust, high fan blade stress (from a distorted velocity profile at the fan face) and core-compressor stall. Therefore, a means must be provided to prevent cowl lip separation (Figure 2). Methods for reducing the severity of the flow condition include rotating (drooping) the lower cowl lip downward, adding an auxiliary inlet, translating the lower cowl lip and boundary layer control. The drooped cowl lip (Figure 3) has been shown (Ref. 2) to improve lip performance at high angle of attack, and the auxiliary inlet & translated lip (Figures 4 & 5) have the potential to provide additional mass flow to the compressor which reduces the flow requirement around the lower cowl lip.

In order to analyze subsonic potential flow about the engine inlet, the Hess panel Method was used to solve the resulting incompressible potential flow problem. The version of the Hess Panel Method that was used could evaluate various configurations of the non-symmetric V/STOL engine inlet.

The current inlet investigation employs a higher order version of the three-dimensional Douglas Program (Ref. 3) which compensates for curved panel surfaces and varying source densities across a panel. Figure 6 (a,b) shows the greater accuracy achieved for the flow surface pressure ratio for an axisymmetric V/STOL inlet by using the higher order panel method over the base method. The base method of the Hess Panel Method assumes all panels are flat and have one constant source density located at the centroid of the panel. Figures 7 and 8 show comparisons between experimental and base method calculations for an additional axisymmetric inlet and a symmetric scoop inlet. The

correlation between the experimental and calculated pressure distributions results in greater accuracy when the higher order method is employed.

HESS PANEL METHOD

The procedure for calculating inviscid incompressible flow about arbitrary configurations is based on a panel method. The higher order Hess Panel Method is the core of the Douglas three-dimensional inlet program which was utilized in this investigation (Ref. 3). This program computes flow about inlets, with or without centerbody or auxiliary inlets. This computation method has been directed toward the numerical solution of Laplace's equation for the computations of four incompressible flow solutions. The four flow solutions are generalized to subsonic flows by the application of certain compressibility corrections. The Hess Panel Method presented in References 4, 5, 6, and 7 is summarized here.

The problem to be solved is that of the steady flow of an incompressible, inviscid fluid past an arbitrary three-dimensional body shown in Figure 9. The flow about the body is determined by the solution of Laplace's equation.

$$\nabla^2 \Phi = 0 \tag{1}$$

Laplace's equation is an exact solution of irrotational, incompressible, and inviscid flow (potential flow) where Φ represents the scalar potential flow fields. The flow is assumed incompressible due to subsonic flow conditions at low Mach numbers. This allows Laplace's equation to be solved without restriction to slender bodies or linearized perturbation flow.

To solve Equation (1) for the scalar potentials, boundary conditions must be specified. The surface of the arbitrary body (denoted by S in Figure 9) is assumed to have an equation of the form:

$$F(x,y,z) = 0 \tag{2}$$

The normal component of the fluid velocity is prescribed on the surface S (F=0) as:

$$\vec{V}\cdot\vec{n}\,\Big|_S = 0 \tag{3}$$

Where $\vec{n}$ is the unit outward normal vector on S, and $\vec{V}$ is the total velocity field vector tangent to the surface. This total velocity vector is determined by Equation (4).

$$\vec{V} = \vec{V}_\infty + \vec{v} \tag{4}$$

Where $\vec{V}_\infty$ is the freestream (onset) velocity, which flows externally across the surface of the three-dimensional body. The onset velocity is assumed to be a steady uniform stream of unit magnitude with isentropic flow along streamlines. The disturbance velocity $\vec{v}$, is the velocity vector on the body. This disturbance velocity opposes the onset velocity and therefore is expressed as the negative gradient of a scalar potential function:

$$\vec{v} = - \text{grad } \phi \tag{5}$$

Substituting Equations (4) and (5) into the boundary condition Equation (3) gives:

$$\left(\vec{V}_\infty - \text{grad } \phi\right)\cdot\vec{n} \Big|_S = 0 \tag{6}$$

Then Equation (7) becomes the boundary conditions for the solution of Equation (1).

$$\text{grad } \phi\cdot\vec{n}\Big|_S = \frac{\partial\phi}{\partial n} \Big|_S = \vec{V}_\infty\cdot\vec{n}\Big|_S \tag{7}$$

A regularity condition at infinity is also required. In the usual exterior problem the condition is:

$$\left|\text{grad } \phi\right| \to 0 \tag{8}$$

Which states that at a distance from the surface the scalar potential flow field is required to be highly three-dimensional due to the complexity in shape of many body disturbances. Therefore the total flow field is defined as:

$$\phi = - \left(x\vec{V}_{\infty x} + y\vec{V}_{\infty y} + z\vec{V}_{\infty z}\right) \tag{9}$$

Where

$$x = \phi_x + \phi' \tag{10a}$$

$$y = \phi_y \tag{10b}$$

$$z = \phi_z \tag{10c}$$

The flow conditions x, y, and z denote three-dimensional flow. Cross flow considerations are accounted for in the y and z terms. Since the dominant flow is in the x direction, a disturbance potential, ϕ', is included in Equation (10a).

Now ϕ will be represented as the potential of a source density distribution over the surface S. Applying the boundary conditions to the Laplace Equation yields a potential at a point P in space with coordinates x, y, and z due to a unit point source located at a point q on the surface S is:

$$\phi = \frac{1}{r(P,q)} \tag{11}$$

where r(P,q) is the distance between the points P and q (Figure 9). Accordingly, the potential at P due to a source density distribution $\sigma(q)$ on the surface S is:

$$\phi = \int\int_S \frac{\sigma(q)}{r(P,q)}\, ds \tag{12}$$

which is the disturbance potential due to the surface. Now ϕ is given by Equation (12) automatically satisfies Equations (1) and (8) for any function σ, simply because the point source potential Equation (11) satisfies these equations. The disturbance potential is now differentiated, and the boundary condition at the surface Equation (7) is applied (Ref. 4). The result is an integral equation for the source density distribution:

$$2\pi\sigma(P') - \int\int_S \frac{\partial}{\partial n}\left(\frac{1}{r(P',q)}\right)\sigma(q)ds = -\vec{n}(P')\cdot\vec{V}_\infty \qquad (13)$$

Where $\partial/\partial n$ denotes differentiation with respect to the outward normal direction from S at P'. This equation is a Fredholm integral of the second kind, and the core of the solution method. After solving Equation (13) for σ, the velocity at any point is obtained by differentiating Equation (12). The velocity is added to that of the onset flow to give the resultant velocity component at the point P'.

Equation (13) is solved by a finite element analysis as follows. The arbitrary body is defined by a set of points lying on the surface, S, which are then used to form quadrilateral elements (panels). The centroid of the quadrilateral is chosen as the control point where the normal velocity is required to vanish. The control point of a panel is where the tangential velocity and pressure are calculated. The conditions of the control point are determined from Equation (13), which is simply of the form:

$$A_i \sigma_i = b_i \tag{14}$$

where represents the coefficient after solving the integral on the left side. The quantity represents the boundary condition with denoting source strengths at each panel. The source strength is the only unknown quantity in Equation (14). The solution for σ is found by forming a 'matrix of influence coefficients' as shown below:

$$\begin{bmatrix} A1 & b1 \\ A2 & b2 \\ \cdot & \cdot \\ \cdot & \cdot \\ An & bn \end{bmatrix} \tag{15}$$

The 1,...,n notation represents the indices for each panel employed. The matrix is solved for the source strengths, σ. This matrix solution illustrates the fact that in subsonic flow all panels influence each other on the body. After solving these linear algebraic equations, the velocity at each control point is obtained by multiplying the induced velocities by the respective value of source density, summing over all elements, and adding the onset flow. The method described is termed the 'base method' of the Hess Panel Method since it is assumed that the strength (source strength) is constant across a panel and that the panels are flat.

The base method version of the Hess Panel Method has been modified to include variable singularity strengths and curved panels. This new method is termed 'higher order' (Ref. 5).

Specifically, the source strength is now assumed to be linearly varying across a panel, and the panels are parabolically curved panels based on the effects of local surface curvature. As described in References 5 and 8, it is consistent to always use a source polynomial of one degree less order than the panel polynomial. The transition from the base method to the higher order method consists of adding terms to the original 'matrix of influence coefficients' to obtain an 'altered matrix of influence coefficients' (Ref. 5).

In order to create the higher order method, five additional integral expressions are required. For a given panel, the coefficient of the integral in the base method contains the unknown values of the source density at the control point of the panel as described previously. In the higher order method, three of the five new integrals have as their coefficients one of the three local curvatures of the surface multiplied by the unknown value of source density. These four integrals are added to obtain a corrected unknown value of source density (a corrected influence coefficient). The other two new integrals have as their coefficients the unknown derivatives of the source density with respect to two orthogonal directions tangent to the panel. On a given panel, the source density variation is expressed in terms of the source density on the adjacent panels in a least-square sense. The result is added to the above corrected influence coefficient to obtain an 'altered influence coefficient'. The preceding is a brief summary of the details presented in Reference 5.

In the Douglas three-dimensional inlet programs, the Hess Panel Method is used to generate four unique fundamental solutions. The four solutions are: 1) 0 degree onset freestream of unit magnitude; 2) 90 degree onset freestream of unit magnitude perpendicular to the horizontal axis of the inlet cross section; 3) 90 degree onset freestream of unit magnitude perpendicular to the vertical axis of the inlet cross section; 4) zero freestream velocity with a doublet surface providing suction inside the inlet. These four solutions are then linearly combined to determine the incompressible flow in and about the inlet at any desired angle of attack, angle of yaw, freestream velocity, and inlet mass flow. To account for the effects of flow compressibility, the Lieblein-Stockman compressibility correction is employed as documented in References 3, 4, and 9.

The Lieblein-Stockman compressibility correction (Ref. 10) is a correlation based on empirical observation. A function has been developed relating the local compressible velocity to the local incompressible velocity. If V_c is the local compressible velocity, V_i is the local incompressible velocity, $\vec{V}_i$ is the average incompressible velocity across the flow area at the point in question, ρ_i is the incompressible density and $\vec{\rho}_c$ is the average compressible density across the flow area, then the correction function is:

$$V_c = V_i \left(\frac{\rho_i}{\vec{\rho}_c} \right)^{V_i/\vec{V}_i} \tag{16}$$

As documented in Reference 10, the application of the above correction function to obtain compressible velocities from incompressible velocities yields generally excellent correspondence with the exact compressible flow.

To validate the accuracy of the three-dimensional program to be used and to show the improvement of the higher order solution, a V/STOL axisymmetric inlet has been modeled (Figure 10). Experimental data has been obtained (Ref. 11) with the inlet operating at high angle of attack where the flow developed is three-dimensional in nature. These results (as shown previously in Figures 6a and 6b) are compared to the calculated results (for both the higher order method and the base method) obtained from an inlet model shown in Figure 11 with a total of 984 panels on a symmetric half. The calculated result using the higher order agrees well with the experimental data, but as expected, for the same number of panels, the base method provides a less accurate result.

MODIFICATIONS TO TEST INLET MODEL

A two-dimensional experimental wind tunnel model is used at NASA Lewis Research Center for subsonic analysis. Figure 12 shows a side view of the test inlet. The inlet is a two compression ramp inlet of capture aspect ratio 0.724 (H/W) and capture area of 836.77 cm^2. The experimental model was designed based on the GE F404 engine. This model includes a variable geometry cowl lip and four auxiliary inlets for subsonic/high angle of attack analysis.

The inlet was designed in four sections (Figure 12). The inlet section, forward inlet section, diffuser section, and adapter flange section are combined to make up the wind tunnel model. The inlet section is 79.50 cm long and consist of the two compression ramps and the variable drooping/translating cowl lip hardware. The cowl lip hardware is scaled from the F-15 inlet system. This section also includes sideplates of different thickness. The right sideplate is scaled from the F-15 and the thick left side is scaled to accommodate model instrumentation. The leading edges of the sideplates are sharp and similar in contour to the F-15 inlet sideplates. The forward auxiliary inlet section is 76.2 cm long and houses the subsonic diffuser ramp and four auxiliary inlets. The auxiliary inlets are of different thicknesses. These different wall thickness values result in different inlet contraction ratios (A_i/A_{th}). The diffuser section is 60.96 cm long and has a transition from a square forward inlet section to a circular interface flange section. This section provides all of the diffusion in the low speed test mode. The interface flange section

connects the inlet to the low speed wind tunnel support system. This mounting enables subsonic analysis to be performed through the inlet.

In order to properly provide an analytical model of the experimental wind tunnel model the Hess Panel Method was employed. The analytical three-dimensional supersonic inlet used in this analysis was modeled by employing panels which defined the dimensions of the inlet. The supersonic inlet is divided into sections to enable reasonable panel densities at all points on the surface. Due to the dimensional complexity of the inlet, certain areas required high panel densities. The most efficient inlet paneling is one that has a panel distribution which provides the required accuracy with the minimum number of panels. Most regions on the inlet body are flat large surfaces which facilitates fewer and larger panels for more accuracy. The latest version of the Hess Panel Method described in Reference 3 is utilized in the investigation.

The analytical supersonic inlet (Figure 13) used in this investigation has a flat, mostly square exterior, a rounded interior with flat ramp surfaces, and a sharp curved lower cowl lip. The interior is a square constant cross-section with rounded corners from x/D of 3.23 downstream from the upper cowl lip highlight to x/D of 5.88 and transitions at this point to a circular cross-section to the rear of the inlet. Located at the rear of the inlet is a doublet surface, which is used to create a 'ring ' vortex during the static solution. Figure 14 (a,b) shows a schematic right side view of the experimental inlet used in the wind tunnel analysis at NASA. In comparison a right side paneled view of the model developed in this investigation is also shown. The plot is somewhat cluttered due to the method used by the

computer code to draw the geometry. The panel plot is created by drawing panels with unit normal vectors facing the viewing location.

The experimental and analytical models are comparatively equal in overall dimension. The inlet section and the forward auxiliary inlet section are basically the same. The inlet section enables the variation in cowl lip drooping angles of 0, 40, and 70 degrees and translation distances of 2, 4, and 6 in. (5.08, 10.16, and 15.24 cm). The details of the drooped and translated cowl lip designs are given in the next section. The forward auxiliary inlet section has the capability of employing auxiliary ports on each side of the inlet. The diffuser section expands outward on the exterior of the experimental model, while the paneled analytical model does not. A transition from a square to round cross section is employed as seen in Figure 15 on both the experimental and analytical model.

In order to develop this analytical model certain modifications needed to be added to the model developed in Reference 12. The previous model was symmetric about the x-z axis, having a thick sideplate on either side. Symmetry was employed to reduce the number of panels on the inlets for greater accuracy with the Hess Panel Method. In this investigation the symmetric inlet was modified into a non-symmetric inlet having a left sideplate and a thin right sideplate. This was done to match the specifications of the NASA wind tunnel model. Developing a non-symmetric inlet increased the number of panels required to describe the inlet and also the computer CPU run time but yielded results that predict flow characteristics through the inlet.

Another modification was the rounding of the exterior corners on the inlet. Figure 15 shows a cross-sectional view of the model that was developed in Reference 12. The view shows the square exterior corners of that reference to be rounded for this investigation. The model now follows the basic existence theorems of the solution method which require that the surface has a continuous normal vector. This requirement is not satisfied when discontinuities in curvature exist such as in a corner. According to Reference 6, the corner can be rounded to maintain a continuous normal vector. A study performed in Reference 12 analyzed the affects of 2, 4, or 6 panels joined together to form a rounded interior corner. The study showed that 4 panels gave better results than 2 panels. The increase to 6 panels slightly improved the results, but not appreciably. From this study a 4 panel distribution was applied to the top two exterior corners on the inlet from a x/D of 0 to 9.29. The rounded exterior corner was produced by creating a 90 degree arc with a 2.946 cm. radius, which is the thickness of the right sideplate. At every 22.5 degrees of the 90 degree arc a panel was produced. This results in 4 panels for the entire arc. The bottom two corners were paneled fitting an ellipse through the y-z plane. An ellipse best described the shape of the two bottom corners and is the geometry specified in the blueprints of the scale model. An ellipse was also employed due to the changing thickness of the corner near the leading edge. The left sideplate adapted well to the ellipse due to the constant changing thickness out to 6.368 cm. from the sideplate leading edge.

The leading edge surface on each sideplate used in Reference 12 transitioned to a sharp point at the edge and did not account for curvature affects. In this study the leading edge was rounded by using an ellipse from the highlight to a distance of 0.28D downstream of the leading edge. Figure 16 (a,b) shows top views of the experimental and analytical model used in this investigation. Figure 16b shows the close modeling employed near the leading edge.

The last modification to the inlet involved making the inlet flexible to various geometry modifications. The geometrical changes result from replacing the lower cowl lip with drooping/translating cowl lips and the inclusion of auxiliary ports. A skeleton geometry consisting of all panel sections not associated with the cowl lips, and auxiliary ports was created. The cowl lip sections are designed to provide droop angles of 0, 40, and 70 degrees and translation distances of 2, 4, and 6 in. (5.08, 10.16, and 15.24 cm). Changing the droop angle simulates rotating the cowl lip about a circular arc element, termed the knee. Translation of the lower cowl lip is achieved by extending the lower lip the desired slot distance, δ, from the pivot location as seen in Figure 17. After the desired droop/translated lip is applied to the skeleton, auxiliary ports or cover plates are incorporated into the forward auxiliary inlet section. Cover plates are located on the interior and exterior of the auxiliary ports to form a constant moldline without auxiliary openings. If auxiliary inlets are desired, they are easily added to the skeleton section. The auxiliary inlets can be placed on all four sides and in any combination.

DESIGN OF FLOW IMPROVEMENT CONCEPTS

In this investigation three concepts for flow improvement were designed for the 2-D supersonic V/STOL inlet model. These three concepts are: 1) a drooped cowl lip, 2) a translated cowl lip, and 3) auxiliary inlets. These concepts are intended to reduce losses associated with separation of flow around a sharp cowl lip at both static and low speed/high angle of attack performance.

Drooped Cowl Lip

To enable better inlet performance under typical V/STOL operating conditions of high angle of attack and low freestream velocity, the lower cowl lip is drooped downward. Drooping the lip reduces the severity of the turn the flow must negotiate for a given angle of attack which has the potential to reduce or eliminate lip flow separation. The design of the drooped cowl lip was based on a balance between reduced lip losses and minimizing lip knee separation. This knee separation is caused by exposing the circular arc segment of the inlet to the flow by drooping the lip. The experimental droop lips used at NASA Lewis were designed based on available data collected in References 2 and 14, and from the MCAIR potential flow analysis (Ref. 15). The MCAIR analysis models the inlet by using surface panels with either source or sink control points located at the centroids of the panels. In this analytical investigation, panel models for 0, 40, and 70 degree cowl lips were developed. Cross section views and the geometry points for the cowl lips are shown in Figure 18. These points represent cowl lips

that are symmetric about the horizontal center line (Ref. 12). To create the 40 and 70 degree droop lip panel models, the lip geometry sections are modified, and additional sections required to complete the side plates at the drooped sections are developed.

Auxiliary Inlets

Auxiliary inlets can be placed on the top, bottom, left, and right sides of the forward auxiliary inlet section. The experimental auxiliary inlets were designed using a 2-D potential flow analysis procedure (Ref. 15). This investigation employs port design auxiliary inlets. Figure 19 (a,b,c) displays various dimensions of the port design. These ports utilize forward and aft-ramps to form the flow passage. This design maximizes the internal flow area for a given cutout in the inlet. Each port is designed to have a throat area of 35% of the main inlet throat area. Using all four auxiliary inlets provides 140% of the main inlet throat area. The radii R_1 and R_2 of both the forward and aft-ramps are held constant for all four auxiliary ports. The aft-ramp thicknesses have different contraction ratios (A_i/A_{th}). Figure 19c shows the calculated contraction ratios which apply to both the experimental wind tunnel model and the analytical model used in this investigation.

The effect of one or more auxiliary inlets on mass flow over the cowl lip can be studied when cover plates are employed. These cover plates close off the mass flow through the auxiliary inlet. The NASA model simply places a cover over the exterior portion of the auxiliary inlet, leaving the interior cavity exposed to internal flow. In this

investigation both the forward and aft-ramps were taken out and sideplates were used to hold a constant mold surface on both the interior and exterior of the main inlet. Four paneled cover plate sections were developed. These cover plates can replace the auxiliary inlets on the top, bottom, left, and right sides.

Translated Cowl Lip

A translated cowl lip provides additional area for the required inlet mass flow; thus, the mass flow over the cowl lip is reduced, and the chance of flow separation on the inlet lip is lessened. The translated cowl lip acts basically the same as the auxiliary ports in that both design modifications relieve the main inlet from having to carry all of the inlet mass flow. The lower cowl lip geometry is modified by translating the lip forward to form 2, 4, and 6 in. (5.08, 10.16, and 15.24 cm) slots. Figure 17 provides a centerline cross-sectional view of the cowl lip geometry before and after translation. As the slot length is increased to 2, 4, and 6 in. (5.08, 10.16, and 15.24 cm), the inlet flow area is increased by 21%, 41%, and 62% of the main inlet throat area, respectively. The translated geometry was developed relative the drooped lip geometry pivot point located from blueprints of the experimental inlet. The translated geometry panels include descriptions of the new inlet interior and exterior surfaces as well as the forward and aft slot surfaces. These panels were made to be interchangeable with the rotated lip geometry panels and the auxiliary inlet panels.

Figures 20, 21 and 22 provide some possible combinations of the lip geometries. Figure 20 shows the lower half of the supersonic inlet with the cowl lip translated and bottom auxiliary inlet included. A supersonic V/STOL inlet with a drooped/translated cowl lip and bottom auxiliary inlet is shown in Figure 21. The three droop cases, 0, 40, and 70 degrees, are shown with a 4 in. (10.16 cm) translation and all auxiliary inlets included in Figure 22.

NUMERICAL MODEL FLOW RESULTS

Parametric studies of many different model configurations were performed to analyze the potential flow results over the lower cowl lip. These configurations were based on variations of the flow improvement concepts incorporated in the model inlet. Flow cases were studied for V/STOL inlet configurations which incorporated the various combinations of auxiliary ports, translation distances, and droop angles. These flow cases were analyzed at 0, 15, and 30 degrees angle of attack, with main inlet cowl lips drooped at 0, 40, and 70 degrees. Freestream Mach numbers of 0.06, 0.12, and 0.18 were employed to study flow characteristics at low speeds. Throughout the study a control station Mach number of 0.45 was used, except when variations in control station Mach number were investigated.

In order to obtain flow results, flow cross sections and a control station were placed in the flow passages of the inlet. Figure 23 (a,b) shows the application of cross sections and control stations. Each cross section spans the interior of the inlet, translation gap, or auxiliary inlet to determine mass fluxes through these openings. One cross section is selected as the control station where the desired flow rate is set. This control station combines the fundamental solution for given freestream conditions and mass flows. In this investigation, the mass flow, pressure, and velocity distribution results around the cowl lip, translated lip aft surface, and auxiliary inlets are of interest.

Comparison with Experimental Results

The calculated surface static pressure along the lower cowl lip for the 0 degree cowl lip model are now compared with experimental surface pressures. The model used incorporated four auxiliary inlets which were all open. The run conditions are an angle of attack of 0 degrees, freestream Mach number of 0.12, and an engine face Mach number of 0.528. The results are shown in Figure 24. Excellent agreement is noted on the exterior surface and at the peak pressure location just inside the highlight. Agreement is not so good for s/D distances greater than 0.15. One possible reason for the region where the results do not correspond precisely is that the exact shape of the surface might not be modeled correctly. There is some discrepancy in the measured surface data of the geometry tested in the wind tunnel as compared to the designed geometry. It is currently felt that if the lip surface can be exactly modeled and a run condition used for which no local flow separation exists, then excellent agreement with experimental results can be obtained.

Droop Lip Performance

The purpose of drooping the lip downward is to minimize flow characteristics which are likely to produce flow separation on the cowl lip. Drooping the lip downward increases the effective contraction ratio, which is a secondary performance improvement. This investigation droops the lip 40 and 70 degrees in order to determine the effectiveness of this concept.

The performance of the inlet, as determined by the higher static pressure on the cowl lip, was greatly improved by drooping the lip. Figure 25 compares droop lip angles of 0, 40, and 70 degrees. The control station is located at an x/D of 5.58 and a cross section location at 3.92 based on the upper cowl lip highlight. The results are shown with plots of surface static pressure to total pressure ratio versus non-dimensional surface distance from the lip highlight, s/D. The non-dimensional surface distance is specified as negative exterior to the highlight and positive interior to the highlight. At a surface distance of 0 (cowl lip highlight) the most dramatic improvement is obtained. The 0 degree sharp droop lip shows a large drop in pressure ratio. This is due to the fact that the stagnation point in the flow is located on the exterior portion of the cowl lip. From the stagnation point, the ingested flow must negotiate a turn about the lower lip highlight at high velocities, which cause large pressure drops at the highlight. As the lip is drooped downward the stagnation point moves closer to the highlight or inside the highlight to the lower cowl lip surface. The drooped lip results in a reduced pressure drop around the highlight. For droop lip angles of 40 and 70 degrees the stagnation point is located on the upper surface of the lower cowl lip, and the low pressure ratio of the 0 degree droop lip which may result in flow separation is avoided. However, a lower pressure ratio exists at the knee location. Thus the flow separation problem may be moved from the lip region to the knee region for the 40 degree and 70 degree droop cowl lips.

Variation in Angle of Attack

Figures 26 and 27 show a comparison between wind tunnel experimental results and numerical results found in this investigation. A direct comparison can not be made due to the difference in the x axis of the two figures. Figure 26 plots data based on cowl stations (in inches) with both external and internal surfaces representing positive distance values. Figure 27 plots s/D distances based on centroidal control points of each panel along a strip with the external surface representing negative numbers and the internal surfaces representing positive distance values.

Experimental results of the NASA wind tunnel model (Ref. 16) are shown in Figure 26. These are static pressure ratio plots analyzing angle of attack effects on 0, 40, and 70 degree droop lips and are shown here for comparative purposes. The run was performed with a freestream velocity of 80 knots and the angles of attack were 0, 45, and 90 degrees. For the 0 degree cowl lip, low static pressure ratios resulted from the internal flow analysis. This indicates that flow across the lip is not attached, as the angle of attack is increased. The 40 degree droop lip internal flow begins to separate at high angle of attack. Between angles of attack of 0 and 45 degrees the flow tends to remain attached. The cowl lip pressure data indicate the flow over the 70 degree lip remains attached over the entire angle of attack range. These experimental results show that the 70 degree droop lip provides the best performance improvement at forward speed.

The results found in this three-dimensional model investigation follow the same trends as the experimental wind tunnel results. Figure 27 shows the effect of angle of attack on the droop lip angle. The run conditions are a control station Mach number of 0.45, freestream Mach number of 0.12 and an angle of attack of 0, 15, and 30 degrees. The severity of the flow condition around the sharp cowl lip is evidenced by the sharp peak in pressure on the 0 degree droop lip surface. At 0 angle of attack, the stagnation point for the 40 degree droop lip is at the highlight, so the peak pressure occurs farther downstream at the knee location. The 70 degree droop lip shows that the flow is accelerating up to the knee for a 0 angle of attack. As the angle of attack is increased, the stagnation point moves farther down the exterior surface for the 0 and 40 degree droop lips, which creates an increase in the pressure ratio drop at the highlight. For the 70 degree lip, the stagnation point moves toward the highlight on the inside surface of the lip as the angle of attack is increased to 30 degrees. Since the stagnation point is still on the interior surface at high angle of attack, the flow is likely attached up to the knee. This observation coincides with the experimental wind tunnel results.

The lip diffusion velocity ratio is a useful parameter in comparing the severity of the flow condition around the lip between various droop angles. It represents a ratio of the maximum to minimum velocity on the lip surface. This ratio provides a measure of the severity of the diffusion the flow must traverse (Ref. 17) from the lip highlight to the diffuser exit. The larger the diffusion ratio, the

more likely the flow will separate. For a 15 degree angle of attack, the 0 and 40 degree droop lips have diffusion velocity ratios of 2.628 and 1.262 respectively. The 70 degree droop lip does not experience diffusion of the flow along the lip at 15 degrees angle of attack because the flow is accelerating up to the knee. When the angle of attack is increased to 30 degrees, the diffusion velocity ratios are 2.910 and 1.522 for the 0 and 40 degree droop lips respectively. A lip diffusion velocity is not applicable for the 70 degree droop lip at 0 and 30 degrees angle of attack due to the stagnation point remaining inside the highlight.

For both the 40 and 70 degree droop lips, the region of the severe flow condition now encompasses the knee region where the lip surface transitions into the flat lower inlet surface. This effect is evidenced by the second dip on the pressure plots for these inlets. Since the objective of this work is to evaluate the lip performance, the knee region has been modeled with a larger panel spacing than that required for accurate local surface flow analysis in this region.

Variation in Freestream Mach Number

Figure 28 shows the effect of freestream Mach number values 0.06, 0.12, and 0.18 on the 0, 40, and 70 degree droop lip surfaces with control station Mach numbers of 0.45. For 0 and 40 degree droop, the stagnation point is outside the highlight and moves closer to the highlight with an increase in freestream Mach number. This is evidenced by the decrease in pressure drop around the highlight region. For the 0 degree droop lip surface, the diffusion velocity ratios are

2.817, 2.628, and 2.434 and the peak Mach numbers are 0.812, 0.624, and 0.472 for freestream Mach numbers of 0.06, 0.12, and 0.18, respectively. The stagnation point for the 70 degree droop lip surface moves from just outside the highlight to inside the highlight with an increase in freestream Mach number. The plots show likelihood of flow attachment for each variation in freestream Mach number for the 70 degree droop lip.

Auxiliary Inlet Performance

The auxiliary inlets are designed to improve static and low speed/high angle of attack performance by reducing the amount of air flow around the main inlet lip. This results in reduced lip velocities and corresponding separation losses. To measure the effectiveness of this concept, variations in droop lip angle, angle of attack, freestream Mach number, and control station Mach number were investigated for model inlets fitted with various auxiliary inlets. Each auxiliary inlet was employed, and its effect on the flow around the lip was analyzed. The following paragraphs will discuss forward and aft-ramp flow characteristics and variations in flow field concepts as observed from the numerical results.

Auxiliary Inlet Forward and Aft-Ramp Analysis

Forward and aft-ramp internal performance results are based on contraction ratio. Figure 29 (a,b) shows surface pressure ratio plots for the forward and aft-ramps respectively. The run conditions consist

of a freestream velocity of 0.12 and a control station Mach number of 0.45. The angles of attack are 0, 15, and 30 degrees, with droop lip angles of 0, 40, and 70 degrees. Internal flow pressure distributions were determined for each auxiliary inlet configuration. Figure 29a shows slight pressure drop as the geometry is varied from the top port case to the right port case. The top auxiliary inlet has the highest contraction ratio of 1.893, while the right inlet has the lowest of 1.237. The pressure profiles for the aft-ramp surface shown in Figure 29b illustrate the worsening likely hood of flow separation to occur with decreasing contraction ratio. The right auxiliary inlet configuration produced the likely flow characteristics that would lead to fully separated flow on the aft-ramp portion. Pressure profile plots show that calculated pressure drops remained the same for all variations in droop lip angle and angle of attack analyzed in this investigation.

Effect of Auxiliary Inlet on Droop Lip

Figure 30 (a,b,c) shows that auxiliary inlets yield small improvements in droop lip performance. Auxiliary inlets reduce the drop in surface pressure ratio for the 0 degree sharp cowl lip. Figure 30a shows that at 30 degrees angle of attack the bottom auxiliary inlet has the most effect in reducing the pressure drop around the lower lip. For onset flow conditions the auxiliary inlets perform almost equally in reducing surface pressure drop. Auxiliary inlets affect the 40 and 70 degree droop lips only at the knee location. The propensity for flow

separation for the 40 and 70 degree droop cases is reduced at the knee due to less mass flow conditions over the lip. But the pressure profile on the interior of the lip is little affected by the type of auxiliary inlet. Figures 30 (b,c) indicate that drooping the lip is the most dominant application for inlet improvement performance.

Effect of Auxiliary Inlet with Variation of Angle of Attack

Figures 31, 32, and 33 show the effect of auxiliary inlets at 0, 15, and 30 degrees angle of attack. These three figures are based on droop lip angles of 0, 40, and 70 degrees respectively. The angle of attack performance of the inlet system is sensitive to the employment of auxiliary inlets for the sharp lip case.Figure 31 shows that when an auxiliary inlet is incorporated, the pressure drop at the lower lip highlight is reduced. The higher the angle of attack, the more sensitive the inlet system is to auxiliary inlet performance. Auxiliary inlets produce little effect on the surface pressure distribution for the 40 and 70 degree droop lips over the entire angle of attack range. The only improvement for the droop lips is at the knee location where a reduction in pressure drop about the knee occurs with the use of auxiliary inlets.

Auxiliary Inlet Performance with Variations in Freestream Mach Number

Figures 34, 35, and 36 show that increases in freestream Mach number have small improvement effects on inlet performance. The run conditions consists of a constant angle of attack of 15 degrees, droop lip angles of 0, 40, and 70 degrees, and a control station Mach number of 0.45. The freestream Mach numbers were 0.06, 0.12, and 0.18. The

results show that auxiliary inlets reduce the surface pressure drop for the 0 degree droop cowl lip case, with increases in freestream Mach number. The 40 and 70 degree droop angles show no sensitivity to freestream Mach number except at the knee location. The auxiliary inlets reduce the pressure drop about the knee as seen before.

Variations in Control Station Mach Number and Auxiliary Inlets

The auxiliary inlets were incorporated to determine their effect on sharp cowl lip surface pressure ratio with variations in control station Mach number. The run conditions consist of control station Mach numbers of 0.15, 0.30, and 0.45. The freestream Mach number was 0.12 with a 0 degree droop lip angle. To measure the effectiveness of this concept, the model was evaluated with all auxiliary inlets closed, all auxiliary inlets open, and the left auxiliary inlet open as performed with the wind tunnel model. Figure 37 (a,b,c) shows the results of varying the control station Mach number for these three cases. The results indicate that keeping all auxiliary inlets open greatly reduces the surface pressure drop over that of the closed auxiliary inlet case. With all inlets open, the sharp cowl lip shows little sensitivity to the variation in the Mach number at the control station.

The contraction ratios are the dominating factors in controlling the sensitivity to the required mass flux. The model with closed auxiliary ports has only a contraction ratio at the main cowl lip entrance. With the addition of auxiliary inlets, the contraction ratio increases. This reduces the propensity for lip separation.

Translated Lip Performance

Translating the lower cowl lip provides an additional mass flow passage into the engine inlet which reduces the amount of air flow around the main inlet lip. The reduced air flow around the lower lip results in improved lower lip boundary layer separation characteristics. Thus, the performance of the V/STOL inlet at low speed/high angle of attack conditions is improved. Translation of the lower lip along with variations in lip droop angle, angle of attack, freestream Mach number, control station Mach number, and auxiliary inlets was studied to determine the effectiveness of lip translation as a flow control alternative. The following is a discussion of the flow characteristics of these different combinations as seen from the numerical results obtained from the Hess Panel Method.

Effect of Translation on Drooped Lip

Figure 38 (a,b,c) shows the effect of only translating the lip for droop angles of 0, 40, and 70 degrees, 30 degrees angle of attack, 0.12 freestream Mach number, and 0.45 control station Mach number. Translation of the drooped lip produced small improvements in performance of the 40 and 70 degree drooped lips. However, lip translations reduce the drop in surface pressure ratio for the sharp, 0 degree cowl lip at the lip highlight. Figure 38a shows that the 6 in. (15.24 cm) translation has the greatest effect in reducing the pressure drop around the highlight of the lower lip. For other flow conditions, the various translations perform almost equally in reducing surface pressure drop. Lip translations produce little effect on the surface

pressure distribution along the surface for the 40 and 70 degree droop. Figure 38 (b,c) indicates that drooping the lower cowl lip is the most dominant application for inlet improvement performance.

Effect of Translation With Variation of Angle of Attack

Figure 39 (a,b,c) shows the effect of lip translation at 0, 15, and 30 degrees angle of attack and a 0 degree drooped lip for a 0.12 freestream Mach number and 0.45 control station Mach number. Improvements in the surface pressure distribution at the lower lip highlight come from the addition of a translated lip in this case. The higher the angle of attack the more severe the pressure drop at the lip highlight; however, the addition of the translated lip raises the minimum surface pressure ratio at the highlight as the translation slot size increases. For each angle of attack there is little change in the pressure ratio at the lip highlight between the various amounts of lip translation greater than zero. The 6 in. (15.24 cm) translation provides the best results for surface pressure ratio.

Translated Lip Performance With Variations in Freestream Mach Number

Figure 40 (a,b,c) shows the effect of lip translation at 15 degrees angle of attack, 0 degree drooped lip, 0.45 control station Mach number and 0.06, 0.12, and 0.18 freestream Mach numbers. As freestream Mach number is increased, the minimum pressure ratio at the lip highlight becomes slightly less severe. Translation raises the minimum pressure ratio at the lip highlight and offers small improvements in the lip interior for all freestream Mach number cases. The 6 in. (12.54 cm) translation provides the best pressure distribution for this case.

Variations in Control Station Mach Number and Translation

The three different lip translations were coupled with various control station Mach numbers to determine their effect on the sharp lower cowl lip surface pressure ratio. Figure 41 shows the results of varying the control station Mach number for the 0 degree drooped lip inlet for an angle of attack of 30 degrees, 0.12 freestream Mach number and control station Mach numbers of 0.15, 0.30, and 0.45. As the control station Mach number is increased, the inlet mass flow increases. Thus, the minimum pressure at the lower lip reduced with increasing control station Mach number. Translating the lower lip raises the minimum pressure at the lower lip highlight and is more effective at the higher control station Mach number. The 6 in. (15.24 cm) translation offers the best overall surface pressure ratio.

Effect of Auxiliary Inlet/Translation at High Angles of Attack

Figures 42 (a,b) and 43 (a,b) give the results of lip translation with and without an auxiliary inlet at 90 degrees angle of attack, 0.12 freestream Mach number, and 0.45 control station Mach number for the 0 and 40 degree drooped inlets. Figure 42 shows results for the various lip translations at 90 degrees angle of attack while Figure 43 shows the results for lip translations at 90 degrees angle of attack when a bottom auxiliary inlet is included. The bottom port was chosen over the other ports because it has the most effect in reducing the pressure drop around the lower lip (see Figure 30). In Figure 42 it can be seen that translating the lip improves the flow conditions around the lower lip highlight for both the 0 and 40 degree drooped inlets. Translating the

lip also offers small improvements over drooping on the lip interior surface. Figure 43 shows that while translating the lower lip, when an auxiliary is included, offers an improvement in the pressure distribution at the highlight, the length of translation offers small improvements at the lower lip highlight, and gives no advantage over drooping at other lip locations. Comparing Figure 42 with Figure 43, it can be seen that the inclusion of the bottom port with the various lip translations improves the pressure distribution at the lower lip highlight and provides little improvement at other lip locations. Again, the 6 in. (15.24 cm) translation has the overall best surface pressure ratio.

Comparison of Translation Versus Drooping

In Figure 44 0, 2, 4, and 6 in. (0, 5.08, 10.16, and 15.24 cm) results for translations for a 0 degree drooped inlet are plotted with those of a non-translated 40 degree drooped inlet for 30 degrees angle of attack, 0.12 freestream Mach number, and 0.45 control station Mach number. It can be seen that the 40 degree droop case has a slightly higher surface pressure ratio than the 6 in. (15.24 cm) translation, 0 degree drooped case at the lower lip highlight. As the flow proceeds to the lip interior the surface pressure ratio for the 40 degree drooped case decreases due to the upcoming knee location.On the lip exterior there is basically no difference between the various cases.

Translatory Aft Ramp Analysis

In Figure 45 the surface pressure distribution about the aft knee surface is plotted as a function of the angular location, θ, for the 2, 4, and 6 in. (5.08, 10.16, and 15.24 cm) translation cases. The angular location, θ, is measured relative to the horizontal line drawn through the pivot point as shown in Figure 17. θ is zero at the horizontal location and 90 degrees at the tangent point where the knee joins the interior duct surface. The curves are for a 40 degree drooped inlet at 0 and 90 degree angles of attack, 0.12 freestream Mach number, and 0.45 control station Mach number. For the 0 degree angle of attack case, the surface pressure ratio decreases as the flow approaches the inlet interior with the 2 in. (5.08 cm) translation showing the best results. In the 90 degree angle of attack case the 6 in. (15.24 cm) translation has the best pressure profile at the beginning. As the flow approaches the interior and surface pressure ratio slightly increases, the 2 in. (5.08 cm) translation shows the better results. There is a small difference between 2, 4, and 6 in. (5.08, 10.16, and 15.24 cm) translations for the 90 degree angle of attack case as flow starts onto the knee, but at all other locations and for both cases, there is little difference between the various translations.

CONCLUSION

Geometry modifications and three flow improvement concepts were incorporated on a 2-D supersonic V/STOL inlet for operation in high angle of attack, low speed conditions. The inlet model consisted of improved paneled sections, which when joined together form an analytical model similar to the wind tunnel model employed at NASA Lewis Research Center. This modified inlet was evaluated at various flow conditions by the use of a computer program developed by McDonnell Douglas. This computer program utilized the Hess Higher Order Panel Method to calculate the incompressible potential flow which is then corrected for the effects of compressibility by an empirical correlation. The program produced surface static-to-total pressure ratios which were used to describe the performance of the inlet with flow improvements concepts incorporated. These improvement concepts consisted of drooping the sharp cowl lip 40 and 70 degrees, translating the lower cowl lip 2, 4, and 6 in. (5.08, 10.16, and 15.24 cm), and incorporating auxiliary inlets to reduce the mass flux on the cowl lip. The inlets with flow improvement concepts were compared to a sharp cowl lip inlet with 0 degree droop, no translation and closed auxiliary ports. The major conclusions found from this investigation are summarized below.

Droop Lips

The drooping of the lip was found to be the most effective flow improvement concept. Conditions which may lead to severe flow separation were encountered on the sharp cowl lip. These flow conditions,

characterized by large surface pressure drops, were reduced when the cowl lip was drooped both 40 and 70 degrees. The 40 degree droop lip experienced flow conditions which may produce flow separation at the highlight for the 30 degree angle of attack case and also at the knee location. Drooping the lip 70 degrees produced flow conditions likely to maintain attached lip flow over the entire angle of attack range. The only region of concern for flow separation for the 70 degree droop lip was at the knee. Overall, with variations in angle of attack and freestream Mach number, the 70 degree drooped lip produced the best flow characteristics over the lip for internal flow.

Auxiliary Inlets

Auxiliary inlets improved inlet flow only for the sharp cowl lip 0 degree droop case and around the knee location for the 40 and 70 degree droop cases. The auxiliary inlets greatly reduced the drop in pressure around the highlight, especially at low angles of attack for the 0 degree droop lip. Auxiliary inlets affected the 40 and 70 degree droop lip results only at the knee location, due to less mass flow through the main inlet. Flow characteristics were not improved on the interior portion of the drooped lip with the addition of auxiliary inlets.

The contraction ratio of the auxiliary inlet is the main factor in auxiliary inlet performance, with the top auxiliary inlet providing the best flow results and the right auxiliary inlet creating the least favorable flow at the auxiliary inlet exit.

Translated Lip

Similar to the auxiliary inlet, the translated lip appeared to be effective only for the sharp 0 degree droop case. The translated lip reduced pressure ratios greatly around the lower lip highlight for the sharp 0 degree and for all angles of attack. Flow conditions on the inlet interior were slightly better than the non-translated case, but there was little difference between the various amounts of lip translation.

The translation distance was the main influence on translated lip performance, with the largest distance (6 in., 15.24 cm) having the best results. However, for the 6 in. (15.24 cm) translated lip inlet, 88% of the lower lip section is extended outside the lower lip housing. Because of this amount of lip extension, structural attachment of the extended lip to the inlet side walls may be difficult. It may be advised to consider the 2 in. & 4 in. (5.08 & 10.16 cm) lip extensions combined with auxiliary inlets to provide the required flow control.

Summary

Drooping the lip 70 degrees will provide a supersonic V/STOL inlet configuration with the necessary flow requirements to operate effectively at low speeds. The only concern regards the pressure profile in the knee region. The addition of auxiliary ports or a translated lower lip to the 70 degree rotated lip would be impractical since only slight flow improvements would result.

Another viable inlet configuration is the 0 degree droop and translated combination. The translated lip offers good pressure

profiles at the lip highlight and lip interior for low speed/high angles of attack flow conditions. From a mechanical standpoint the extension of the lower lip axially would seem an easier task than would the rotation of the lip for the droop case. There would also seem to be less stress on a translated lip than on the droop lip due to flight conditions. The addition of auxiliary inlets for this configuration is also impractical, for auxiliary inlets offer no significant improvement to the pressure distribution along the lower cowl lip surface.

A third inlet configuration is the 0 degree droop and auxiliary inlet combination. The results for this case are similar to that of the translated lip combination above, though slightly less advantageous.The auxiliary inlet combination differs from the translated lip combination only in that the extra opening for mass flow is further downstream. There seems to be no advantage or disadvantage to either of these geometry modifications, therefore the translated combination is preferred due to a better pressure profile.

In conclusion, the effective lower lip for supersonic V/STOL aircraft operating at subsonic speeds and high angles of attack may be a modified geometry consisting of a 4 in. (10.16 cm) translated lip and an auxiliary inlet. This geometry combination provides flow improvement about the lower cowl lip equivalent to the 0 degree droop inlet with the 6 in. (15.24 cm) translation or the 70 degree droop inlet.

REFERENCES

1. Research on a Two-Dimensional Inlet for a Supersonic V/STOL Propulsion System (Experimental Data) NASA Lewis Research Center. McDonnell Aircraft Company.

2. Lotter, K. and Malefakis, J.: Intake Design and Intake/Airframe Integration for a Post-Stall Fighter Aircraft Concept. A GRAD Symposium on High Angle of Attack Aerodynamics. Sandefjord, Norway. Oct. 1978.

3. Hess, J. L.; and Friedman, D. M.: Calculation of Compressible Flow In and About Three-Dimensional Inlets With and Without Auxiliary Inlets by a Higher-Order Panel Method. NASA CR-168009, (McDonnell Douglas Report No. MDC J2548), Oct. 1982.

4. Hess, J. L.; and Smith, A. M. O.: Calculation of Potential Flow About Arbitrary Bodies. Progress in Aeronautical Sciences. Vol. 8, pp. 1-138, Pergamon Press, New York, 1967.

5. Hess, J. L.: Status of a Higher-Order Panel Method for Non-lifting Three-Dimensional Potential Flow. McDonnell Douglas Report No. MDC J7714-01, Aug. 1977.

6. Hess, J. L.; and Smith, A. M. O.: Calculation of Nonlifting Potential Flow About Arbitrary Three-Dimensional Bodies. Journal of Ship Research, Vol. 8, No. 2, pp. 22-44, Sept. 1964.

7. Hess, J. L.: The Problem of Three-Dimensional Lifting Potential Flow and its Solution by Means of Surface Singularity Distribution. Computer Methods in Applied Mechanics and Engineering, Vol. 4, No. 3, pp. 283-319, 1974.

8. Hess, J. L.: Constant Velocity and Potential Expansions for Higher-Order Singularity Methods. McDonnell Douglas Report No. J6911, June 1975.

9. Hess, J. L.; Mack, D. P.; and Stockman, N. O.: An Efficient User-Oriented Method for Calculating Compressible Flow In and About Three-Dimensional Inlets. NASA CR-159578, (McDonnell Douglas Report No. MDC J8497), April 1979.

10. Lieblein, S.; and Stockman, N. O.: Compressibility Correction for Flow Solutions. Journal of Aircraft, Vol. 9, No. 4, April 1972.

11. Burley, R. R. and Hwang, D. P.: Experimental and Analytical Results of Tangential Blowing Applied to a Subsonic V/STOL Inlet. NASA TM-73728, 1982.

12. Boles, M. A.; Branscomb, C. S.: Theorectical Evaluation of Engine Inlet Drooping Cowl Lip Designs For Supersonic V/STOL Aircraft. North Carolina State University, October 1984.

13. NASA Lewis Research Center: Two-Dimensional Inlet Model for Navy Type B V/STOL Tests in Lewis Research Center Wind Tunnels. Contract NAS3-22158, September 1979.

14. Bristow, D. R.: Modification of the Douglas Neumann Program to Improve Efficiency of Predicting Component Interference and High Lift Characteristics. NASA CR-3020, August 1978.

15. Research on a 2-D Inlet for a Supersonic V/STOL Propulsion System (Results) NASA Lewis Research Center.

16. Boles, M. A.; and Stockman, N. O.: Use of Experimental Separation Limits in the Theoretical Design of V/STOL Inlets. Journal of Aircraft, Vol. 1, No. 1, Jan. 1979.

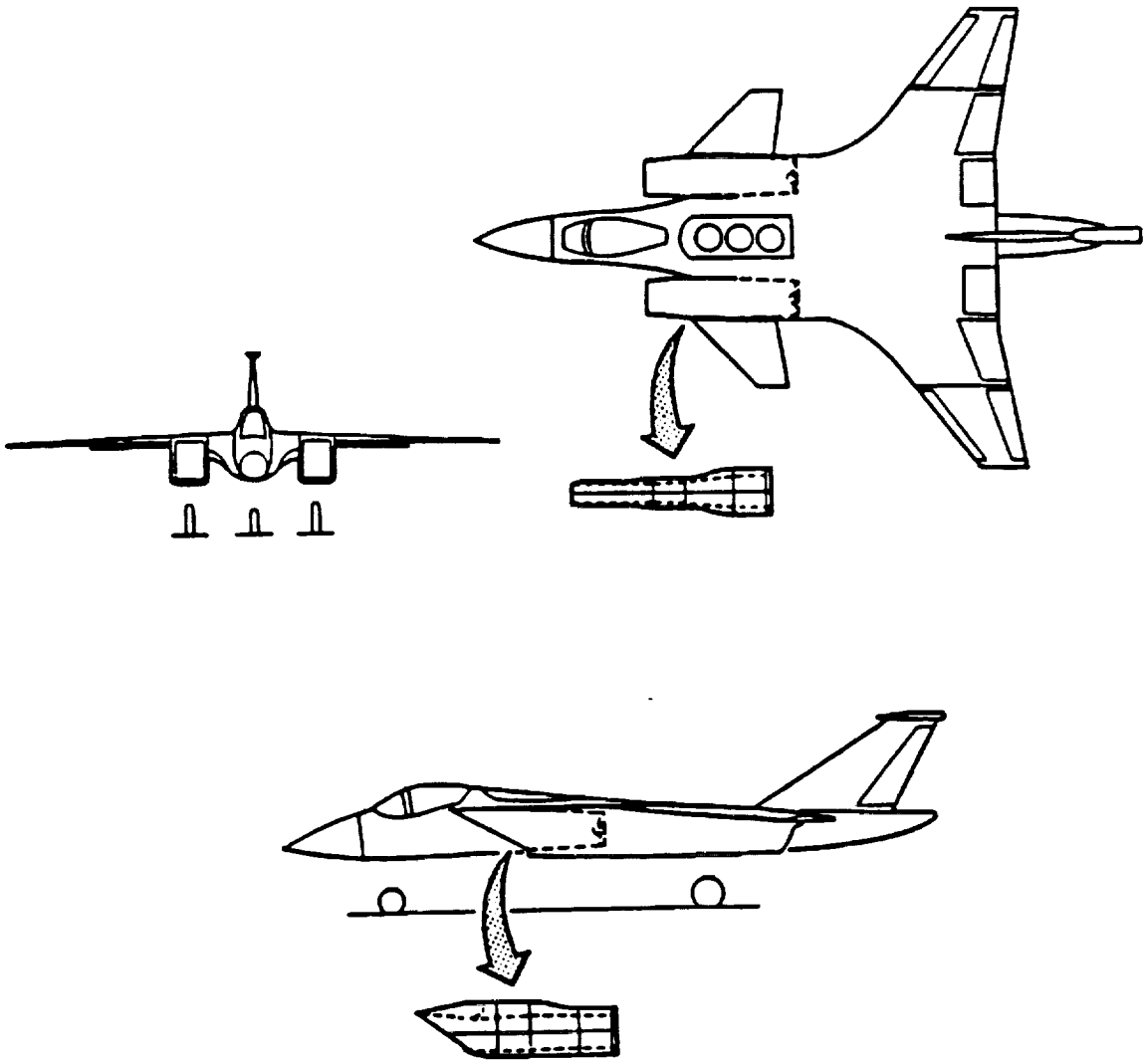

Figure 1. A typical supersonic V/STOL aircraft configuration.

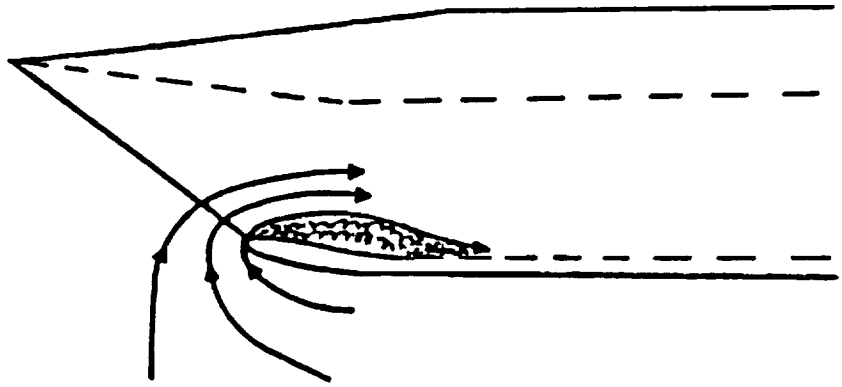

a) Static flow condition.

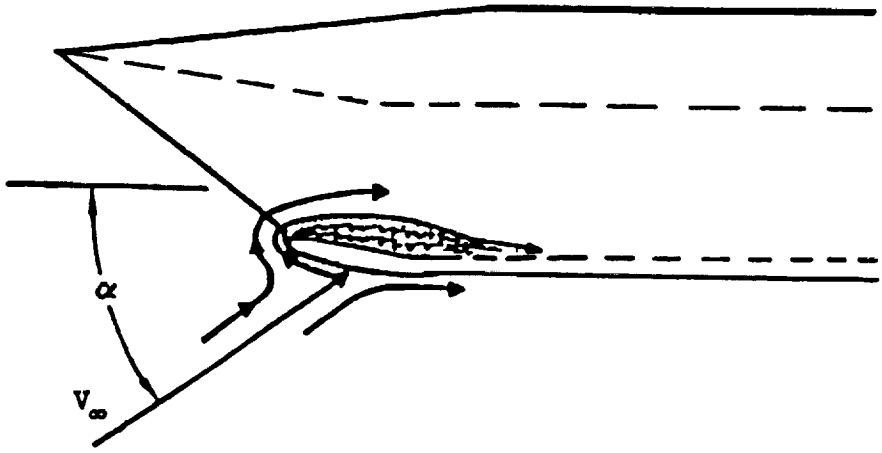

b) Angle of attack flow condition.

Figure 2. Lower cowl lip separation on a supersonic V/STOL inlet.

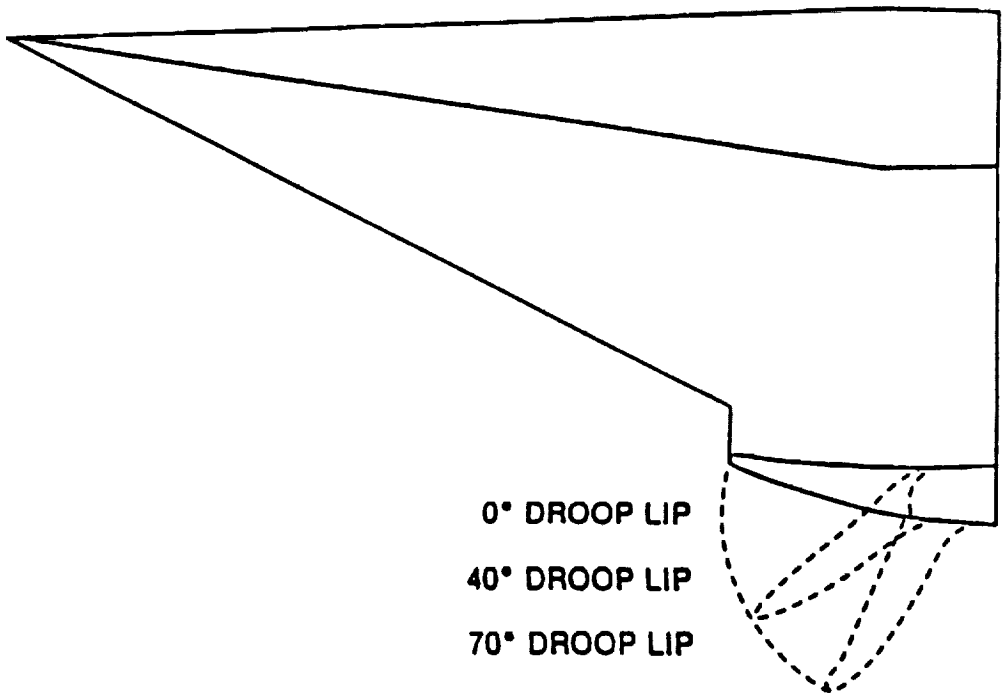

Figure 3. Drooping lower cowl lip of the two-dimensional V/STOL supersonic inlet.

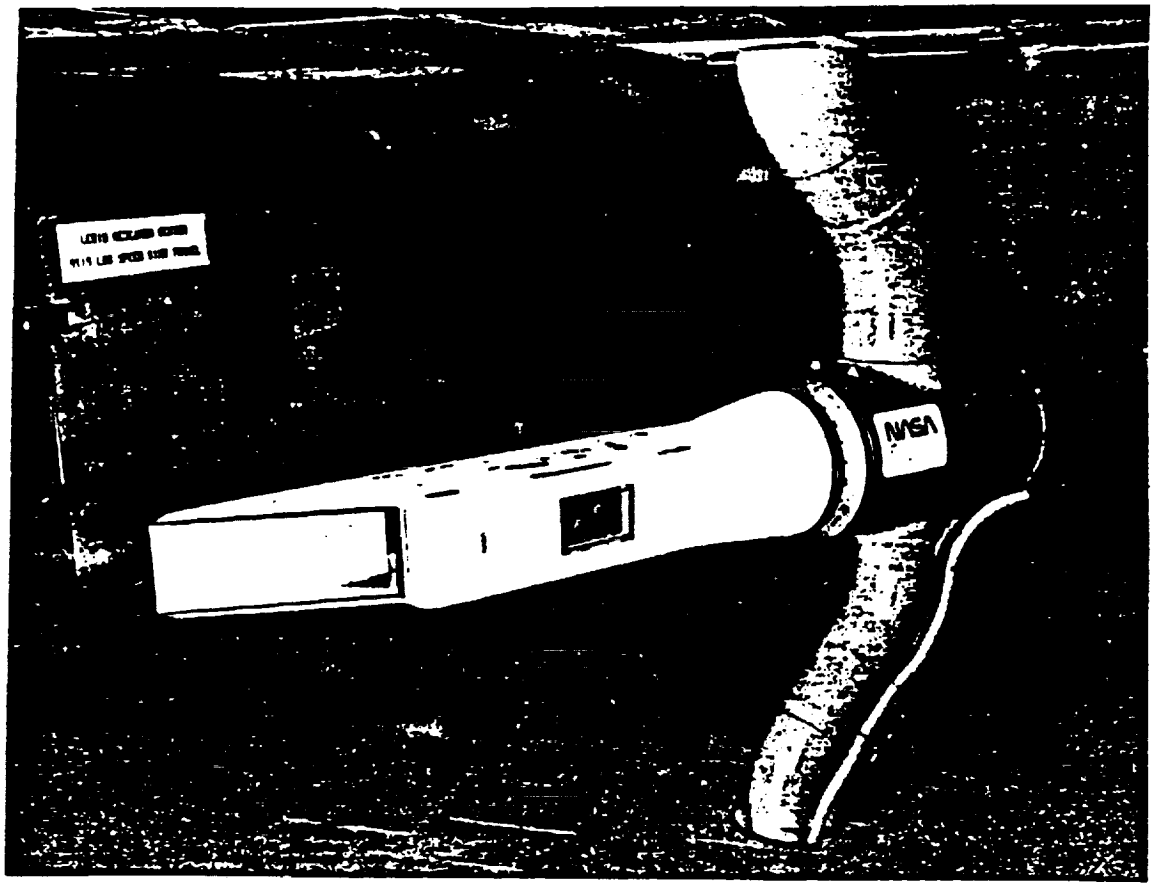

Figure 4. Experimental model of a V/STOL supersonic engine inlet with an auxiliary inlet.

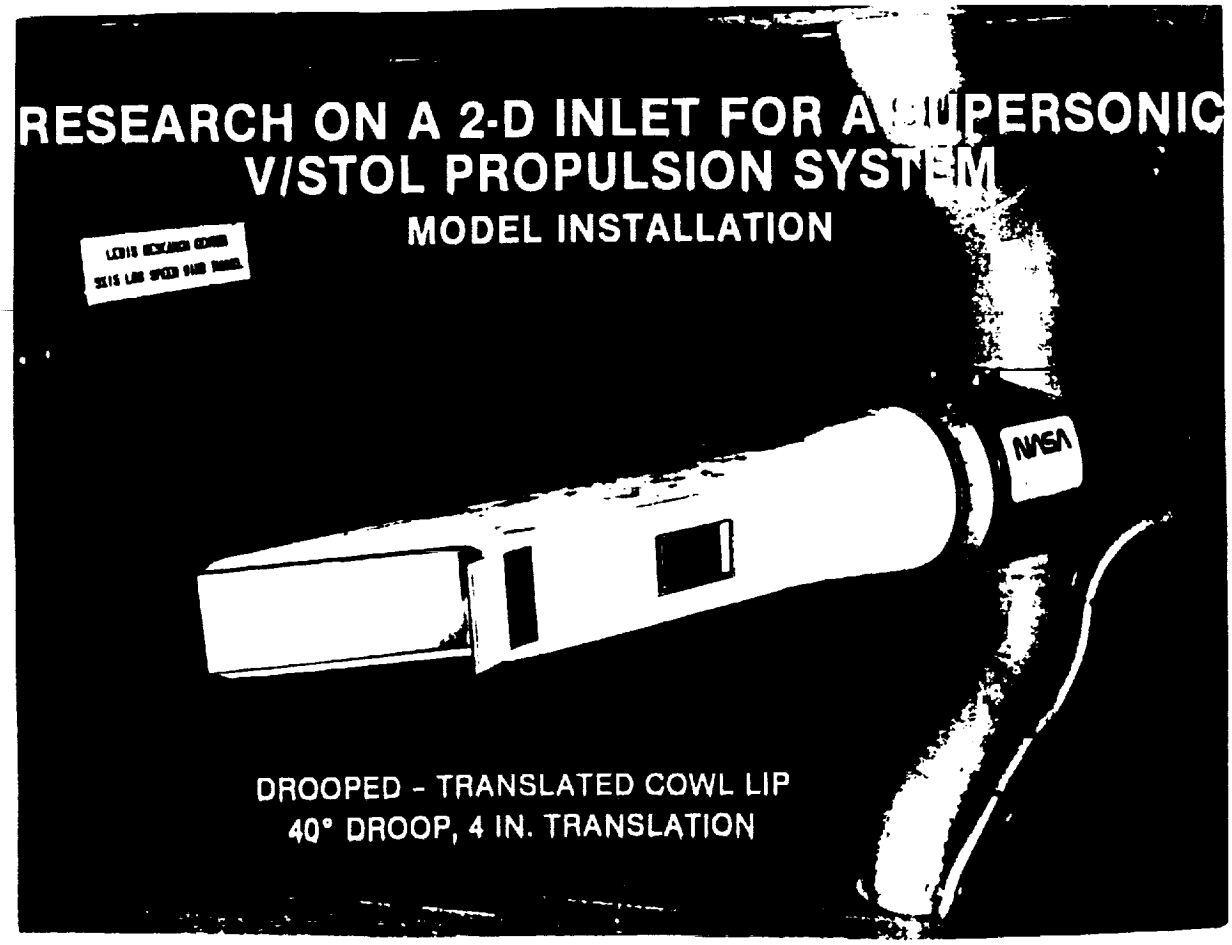

Figure 5 . Experimental model of a V/STOL supersonic engine inlet with drooped/translated lower cowl lip and an auxiliary inlet.

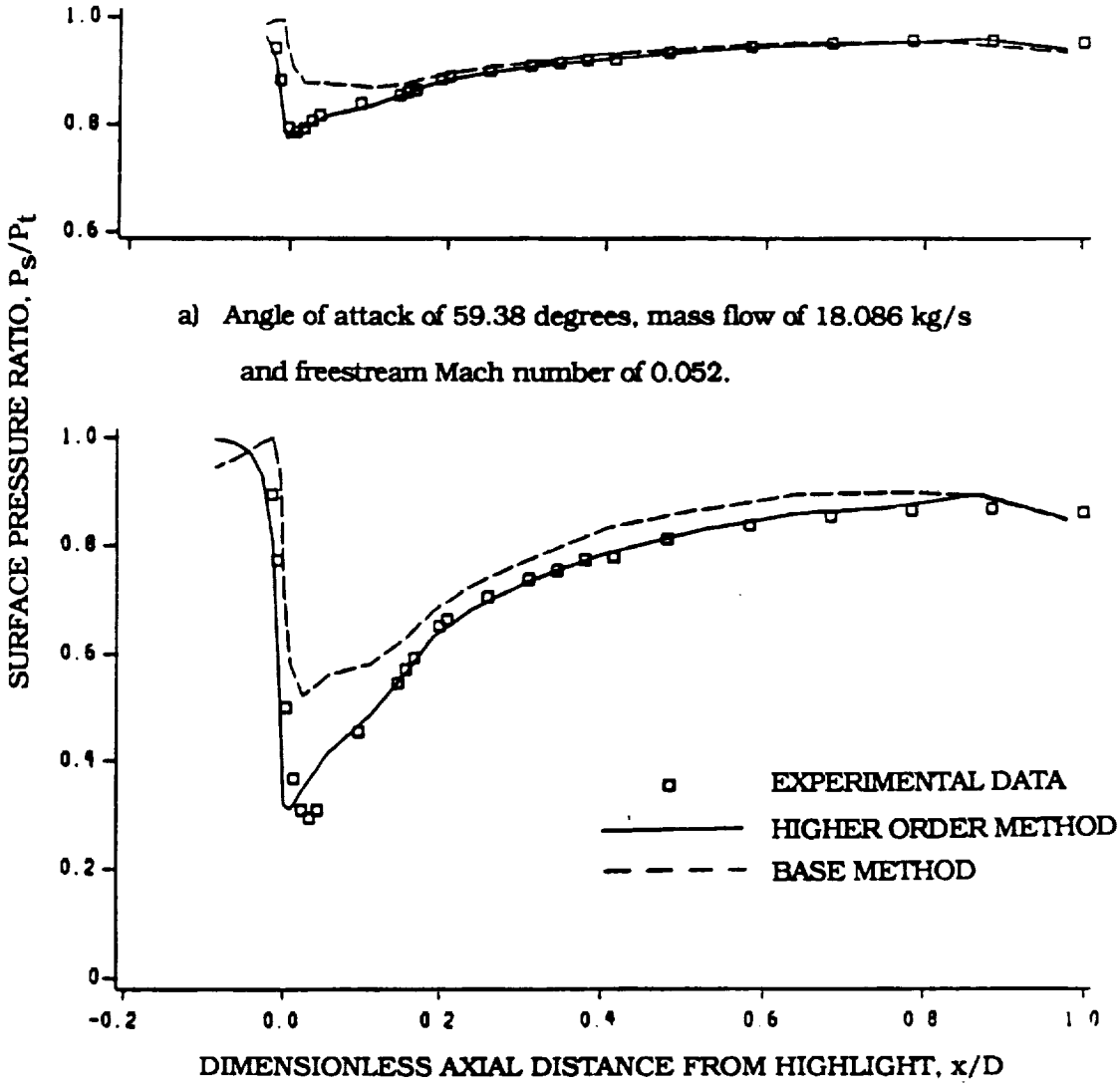

a) Angle of attack of 59.38 degrees, mass flow of 18.086 kg/s and freestream Mach number of 0.052.

b) Angle of attack of 44.546 degrees, mass flow of 27.692 kg/s and freestream Mach number of 0.184.

Figure 6 . Comparison of the three-dimensional potential flow calculations and experimental results for the axisymmetric V/STOL inlet.

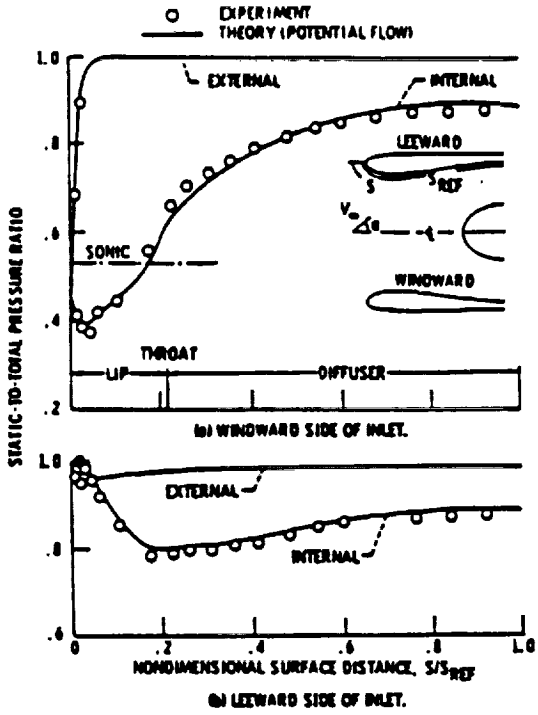

Figure 7 . Comparison of axisymmetric potential flow calculations with experimental results for an axisymmetric V/STOL inlet.

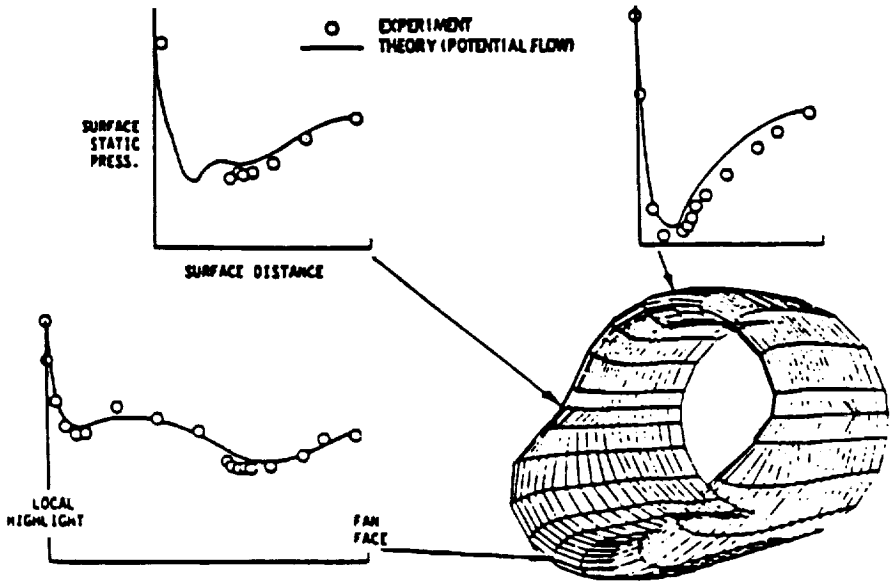

Figure 8 . Comparison of calculated and experimental pressure distributions inside a scoop inlet.

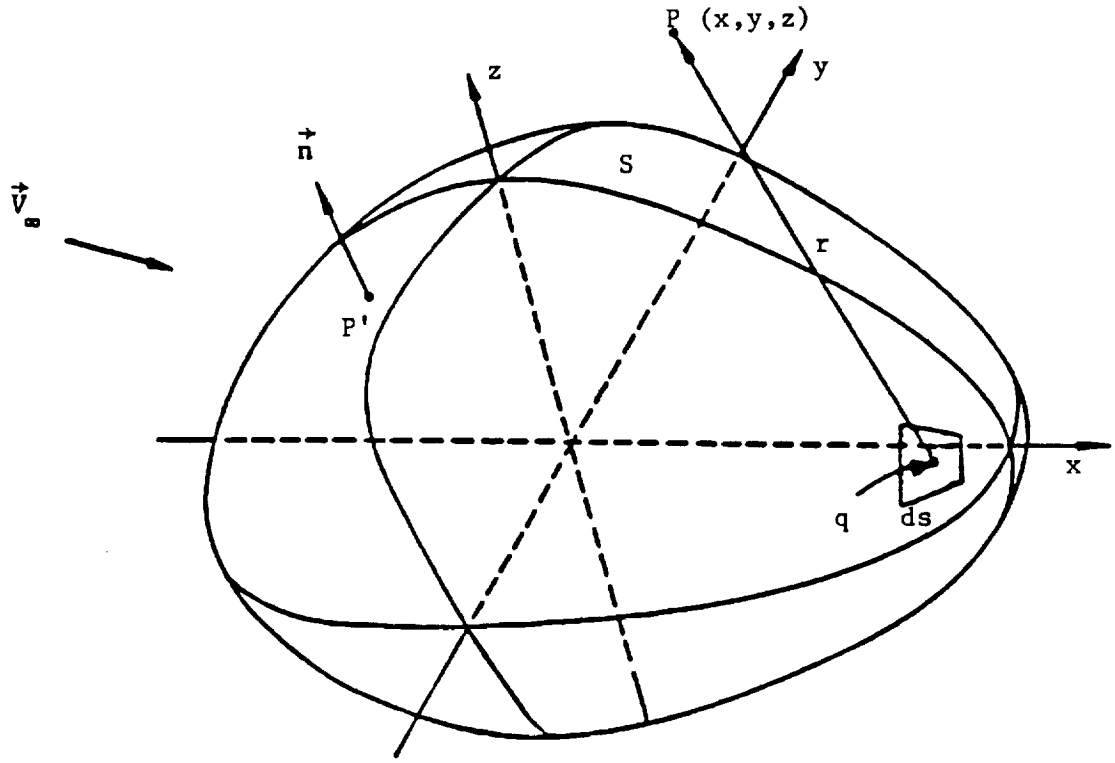

Figure 9 . Arbitrary three-dimensional body.

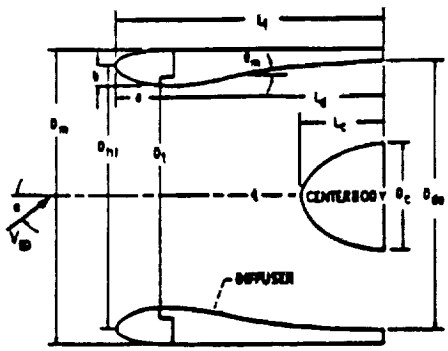

INTERNAL LIP CONTRACTION RATIO, $(D_{hl}/D_1)^2$	1.46
EXTERNAL FOREBODY DIAMETER RATIO, D_{hl}/D_{∞}	0.909
INTERNAL LIP ELLIPSE PROPORTIONS, a/b	2.0
RATIO OF OVERALL INLET LENGTH TO DIFFUSER EXIT DIAMETER, L_1/D_{∞}	1.00
RATIO OF EXIT FLOW AREA TO INLET FLOW AREA, $(D_{\infty}^2 - D_c^2)/D_1^2$	1.21
RATIO OF DIFFUSER LENGTH TO EXIT DIAMETER, L_d/D_{∞}	0.625
RATIO OF CENTERBODY DIAMETER TO DIFFUSER EXIT DIAMETER, D_c/D_{∞}	0.400
MAXIMUM LOCAL WALL ANGLE, θ_{max}, deg	8.7
RATIO OF CENTERBODY LENGTH TO DIFFUSER LENGTH, L_c/L_d	0.357

Figure 10. Axisymmetric V/STOL inlet geometry with an inlet length L_1 of 50.8 cm.

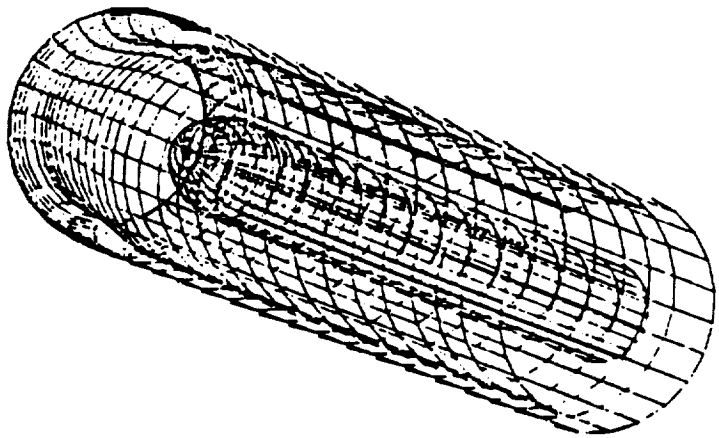

Figure 11. Three-dimensional panel model of the axisymmetric V/STOL inlet.

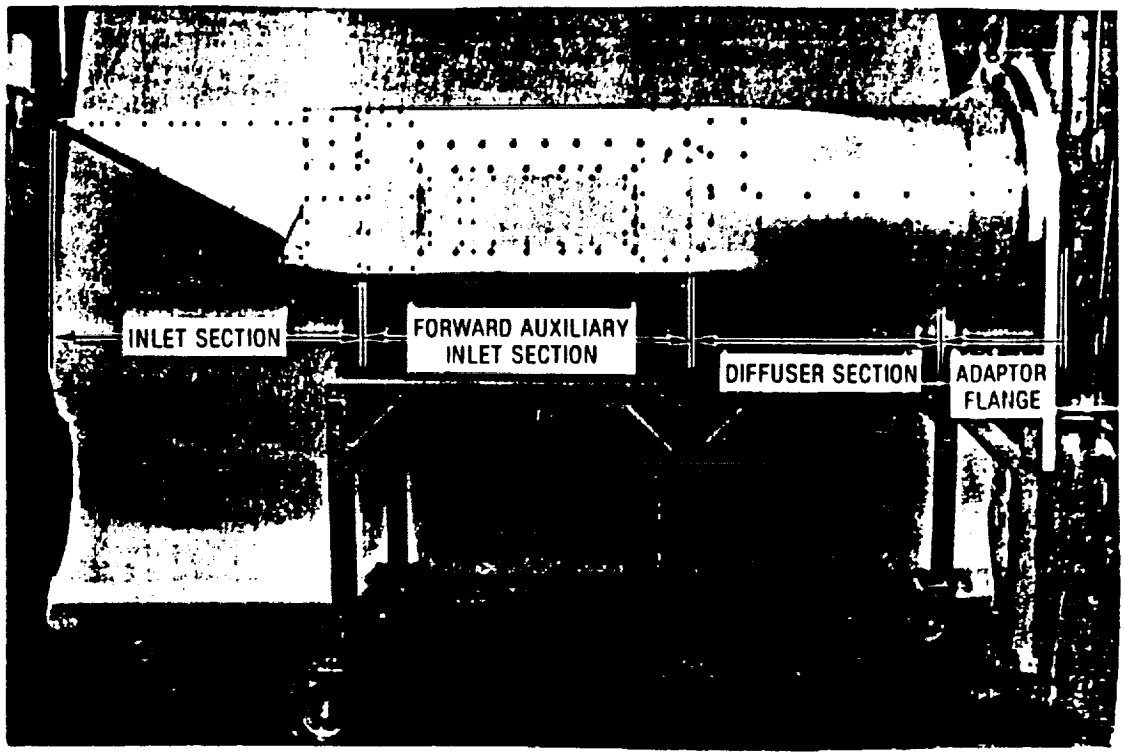

Figure 12. Experimental wind tunnel model.

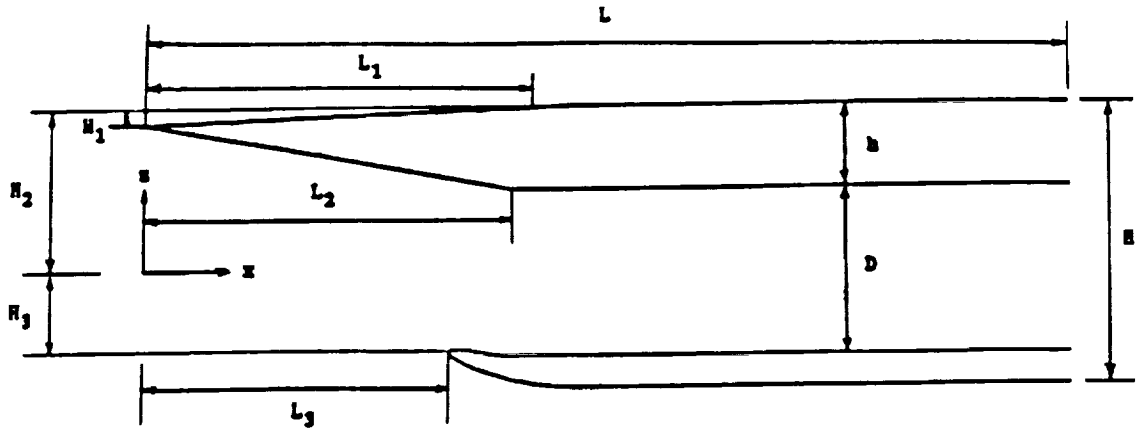

D	24.6 cm
H / D	1.698
H_1 / D	0.103
H_2 / D	1.006
H_3 / D	0.479
L / D	9.292
L_1 / D	3.231
L_2 / D	2.865
L_3 / D	2.354
h / D	0.506

Figure 13. Two-dimensional V/STOL supersonic inlet geometry.

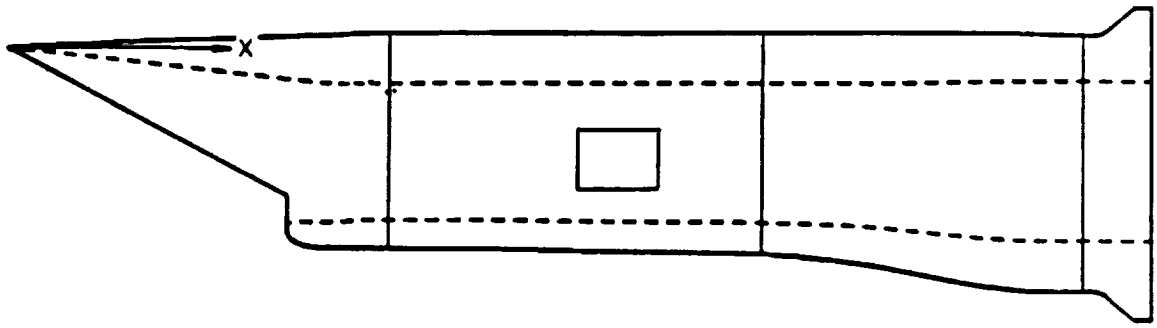

a) Right side schematic view of experimental model.

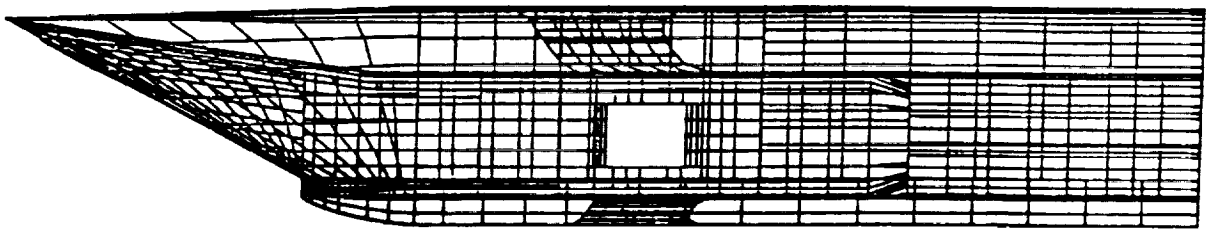

b) Right side paneled view of analytical model.

Figure 14. Comparison of experimental and analytical models with auxiliary inlets.

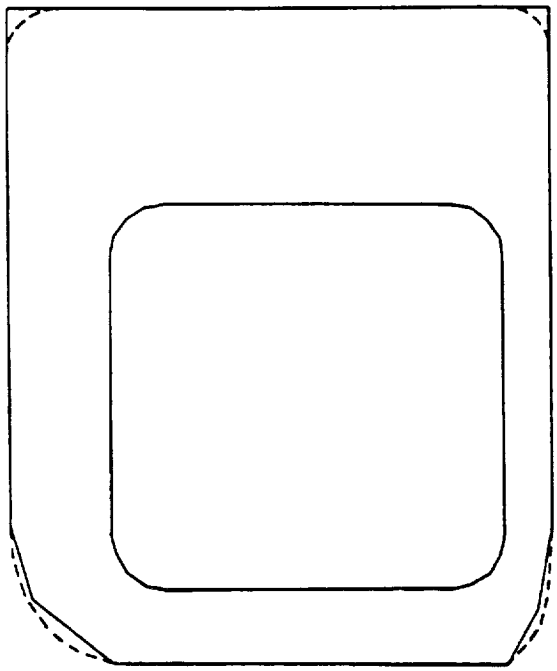

——— Reference 12 model

- - - - - Corner modifications

Figure 15. Modification of inlet by rounding exterior corners.
Frontview at x of 91.44 cm.

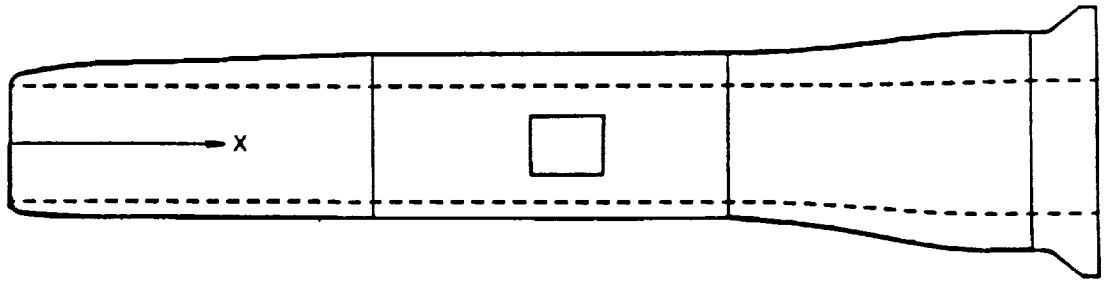

a) Top schematic view of experimental model.

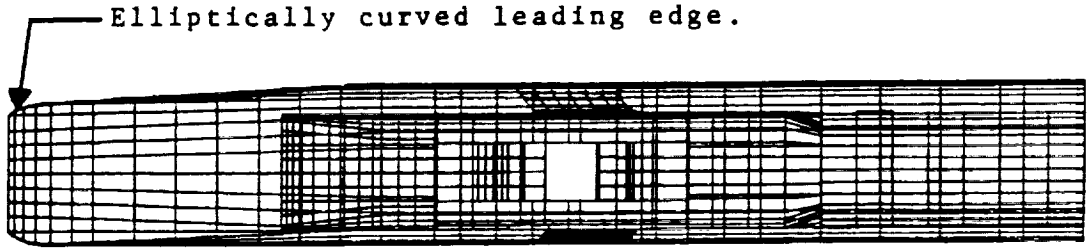

b) Top paneled view of analytical model.

Figure 16. Comparison of experimental and analytical models with auxiliary inlets.

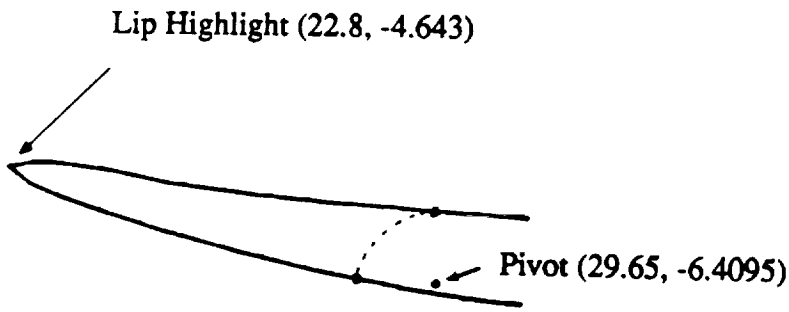

BEFORE TRANSLATION

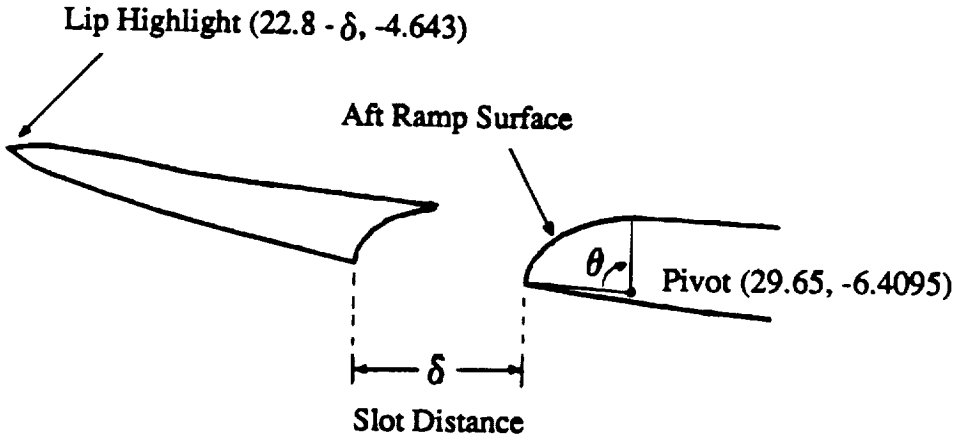

AFTER TRANSLATION

Figure 17 . Translated lower cowl lip geometry for V/STOL supersonic engine inlet.

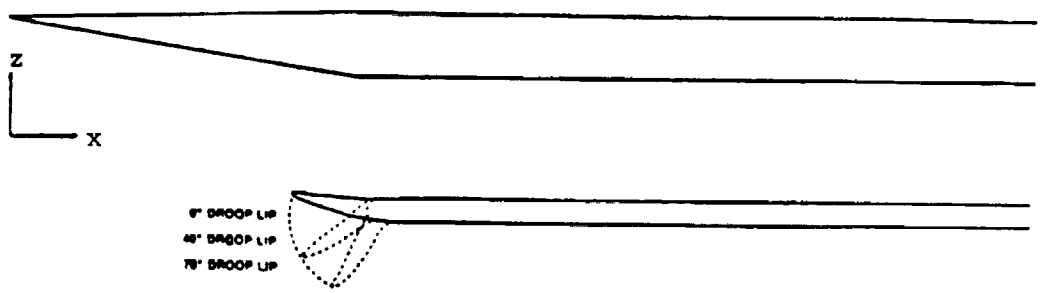

0° DROOP		40° DROOP		70° DROOP	
x / D	z / D	x / D	z / D	x / D	z / D
31.3000	-4.8430	31.3000	-4.8430	31.3000	-4.8430
30.5300	-4.8530	30.5300	-4.8530	30.5300	-4.8530
29.3801	-4.8688	29.5637	-5.0634	29.5637	-5.0700
28.5792	-4.8739	28.5973	-5.3866	28.3368	-6.2800
27.7375	-4.8573	27.9871	-5.9053	28.0677	-6.8016
26.8584	-4.8237	27.3316	-6.4336	27.7642	-7.5869
25.9500	-4.7689	26.6366	-6.9730	27.4320	-8.4015
25.5000	-4.7230	25.9055	-7.5149	27.0698	-9.2364
25.0000	-4.6455	25.5313	-7.7690	26.8728	-9.6435
24.5000	-4.5680	25.0984	-8.0310	26.6289	-10.0869
24.0000	-4.5130	24.6656	-8.2930	26.3851	-10.5302
23.7500	-4.5030	24.2472	-8.5723	26.1624	-10.9813
23.5000	-4.5019	24.0493	-8.7253	26.0675	-11.2127
23.2499	-4.5029	23.8571	-8.8852	25.9810	-11.4473
23.0000	-4.5279	23.6662	-9.0467	25.8964	-11.6826
22.9001	-4.5531	23.4908	-9.2265	25.8344	-11.9260
22.8500	-4.5690	23.4304	-9.3100	25.8238	-12.0285
22.8000	-4.6430	23.4115	-9.4432	25.8741	-12.1533
22.9000	-4.8030	23.5910	-9.5015	26.0587	-12.1141
22.9999	-4.8630	23.7061	-9.4832	26.1492	-12.0407
23.2500	-4.9980	23.9844	-9.4259	26.3616	-11.8519
23.5000	-5.1130	24.2499	-9.3533	26.5552	-11.6563
23.7500	-5.2180	24.5089	-9.2730	26.7393	-11.4572
24.0008	-5.3169	24.7646	-9.1876	26.9181	-11.2554
24.5000	-5.4930	25.2602	-9.0016	27.2543	-10.8465
25.0000	-5.6478	25.7427	-8.7988	27.5708	-10.4297
25.4996	-5.8027	26.2250	-8.5963	27.8872	-10.0131
25.9500	-5.9217	26.6465	-8.3980	28.1531	-9.6307
26.8583	-6.1323	27.4777	-7.9754	28.6616	-8.8491
27.7375	-6.3166	28.2697	-7.5515	29.1356	-8.0860
28.5791	-6.4644	29.0094	-7.1237	29.5623	-7.3456
29.3800	-6.5719	29.6920	-6.9300	30.0666	-7.0000
30.5300	-6.6649	30.5300	-6.8500	30.5300	-6.8500
31.3000	-6.7050	31.3000	-6.7050	31.3000	-6.7050

Figure 18. Lower cowl lip geometry at the centerline cross section for 0, 40, and 70 degree droop angles.

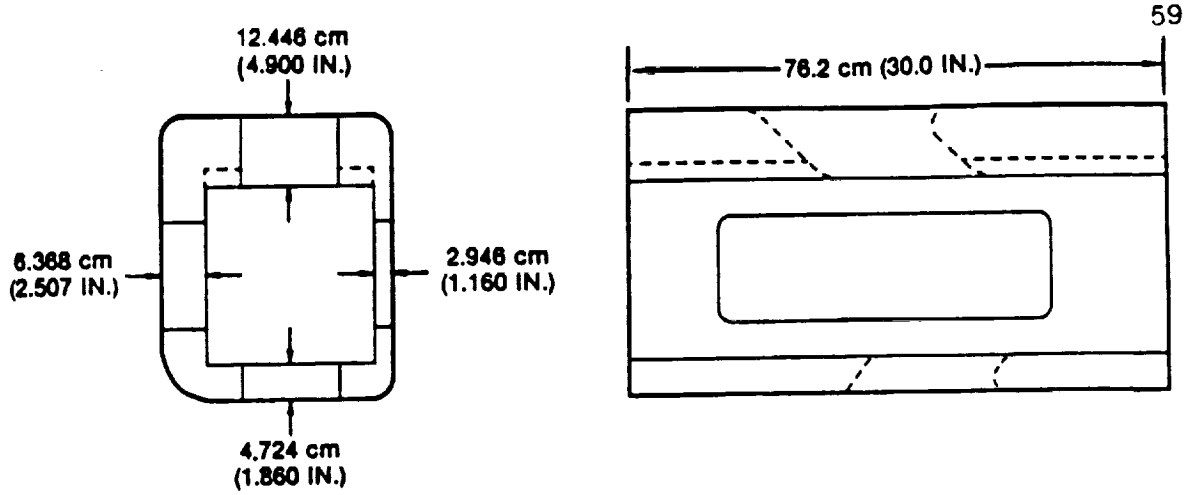

a) Forward auxiliary inlet section.

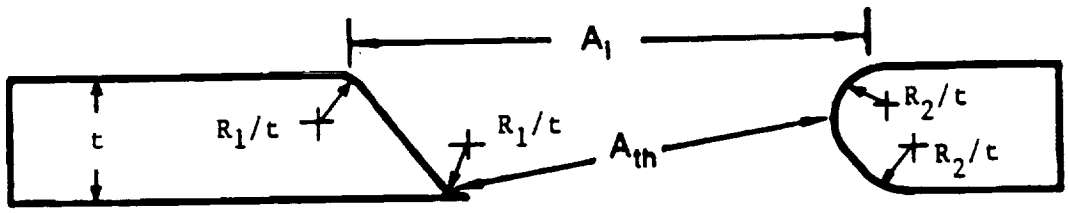

b) Port auxiliary inlet.

AUXILIARY INLETS					
LOCATION	A_i	A_{th}	CR	R_1/t	R_2/t
TOP	404.2 cm^2	213.5 cm^2	1.893	0.08	0.10
LEFT	315.7 cm^2	213.5 cm^2	1.478	0.15	0.20
BOTTOM	290.9 cm^2	213.5 cm^2	1.362	0.20	0.27
RIGHT	264.1 cm^2	213.5 cm^2	1.237	0.33	0.43

c) Auxiliary inlet dimensional data.

Figure 19. Forward auxiliary inlet section.

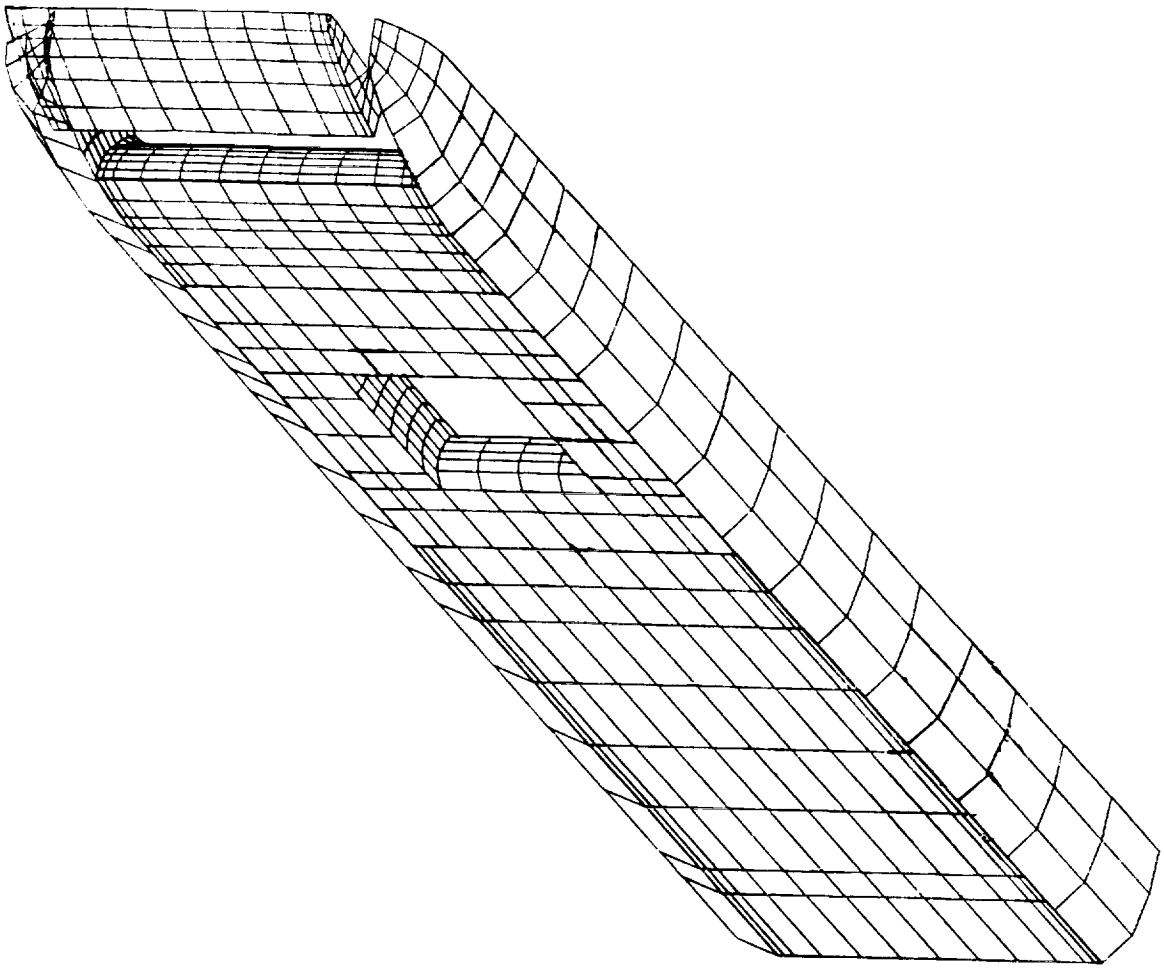

a) Isometric view of lower half of 0 degree droop supersonic V/STOL inlet.

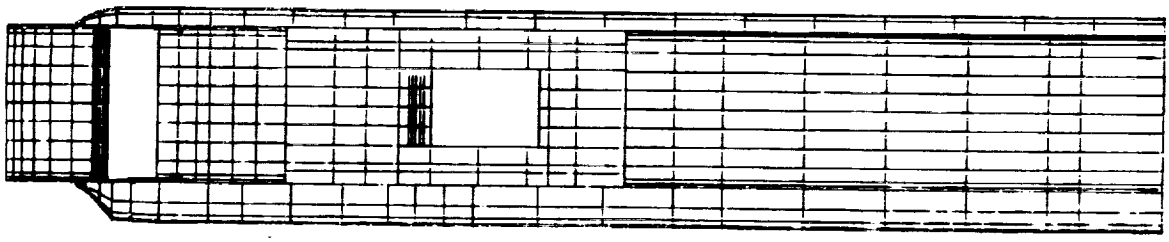

b) Bottom view of lower half of 0 degree droop supersonic V/STOL inlet.

Figure 20. Isometric and bottom view of the lower half of the supersonic V/STOL inlet with bottom auxiliary port included.

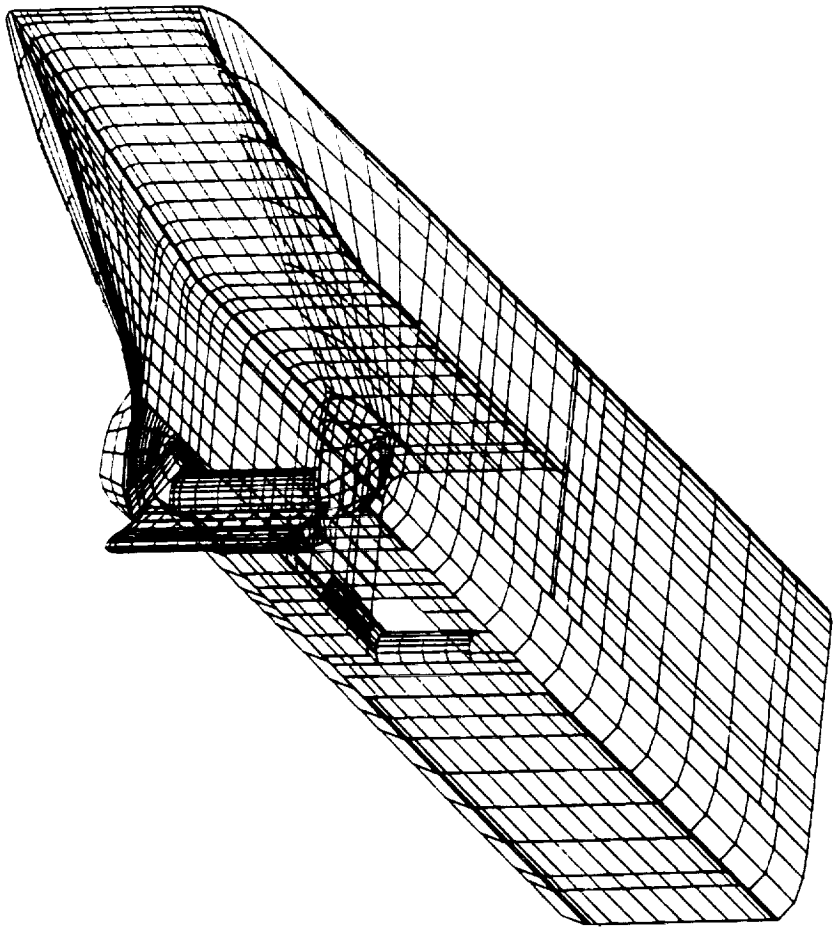

a) Isometric view of 40 degree droop supersonic V/STOL inlet.

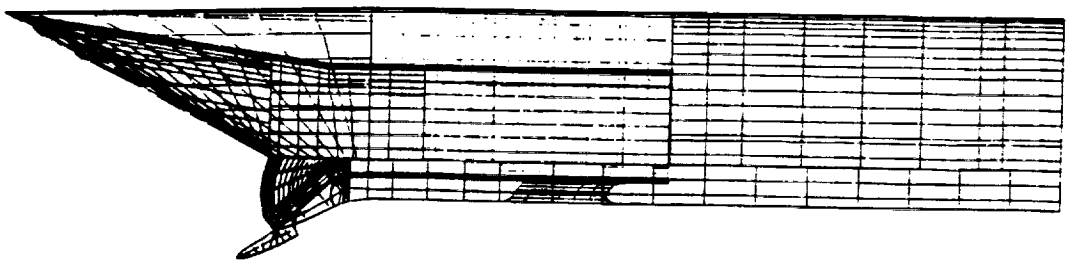

b) Side view of 40 degree droop supersonic V/STOL inlet.

Figure 21 . Isometric and side view of supersonic V/STOL inlet at 40 degree droop and 4 in. (10.16 cm) translation with bottom auxiliary port included.

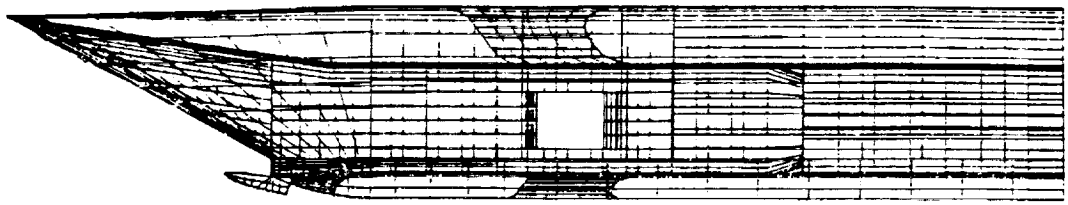

a) 0 degree droop supersonic V/STOL inlet.

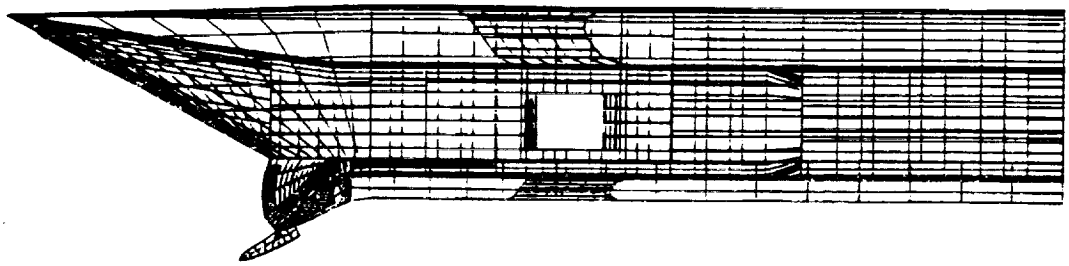

b) 40 degree droop supersonic V/STOL inlet.

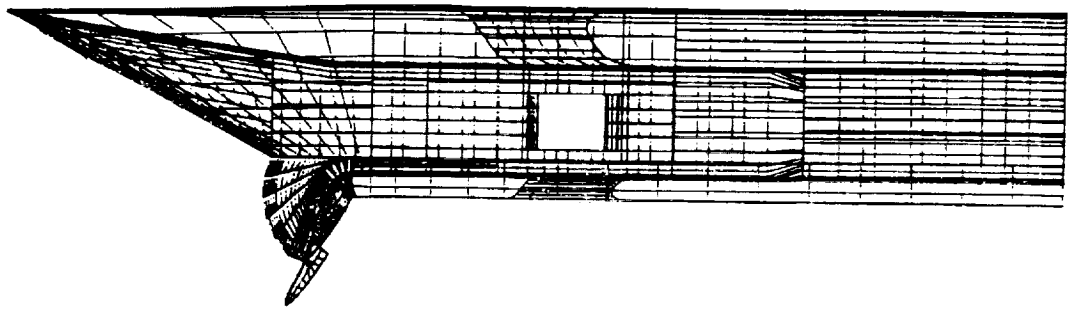

c) 70 degree droop supersonic V/STOL inlet.

Figure 22 . Side view of supersonic V/STOL inlet geometry for 0, 40, and 70 degree droop cowl lips with 4 in. (10.16 cm) translation and all auxiliary ports included.

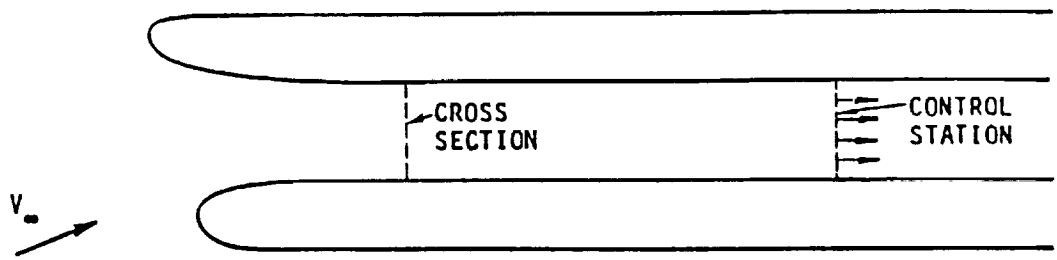

a) Cross section and control station in an inlet.

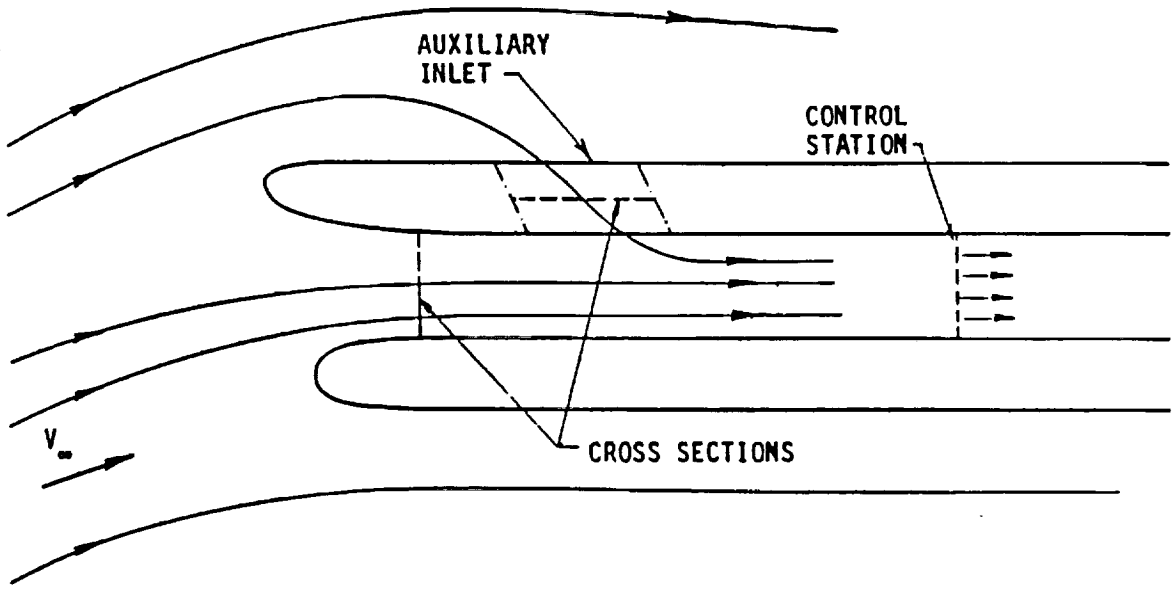

b) Main inlet with auxiliary inlet.

Figure 23. Application of cross sections and control stations.

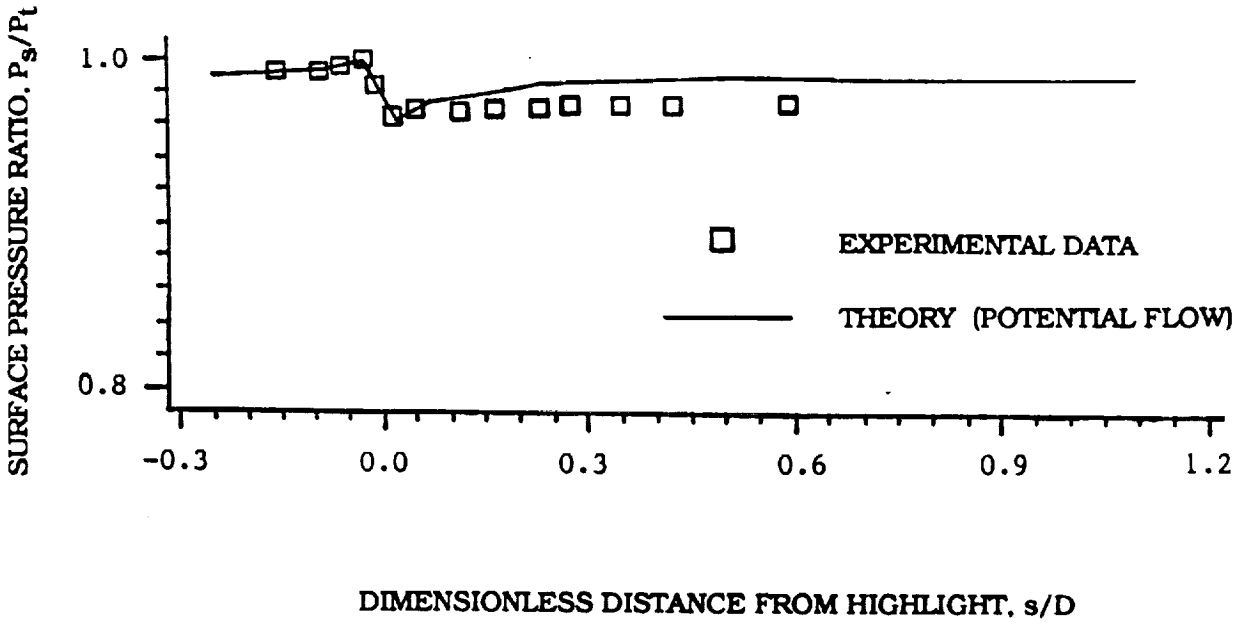

Figure 24. Comparison of three-dimensional potential flow calculations with experimental results for the sharp cowl lip supersonic V/STOL inlet with all auxiliary inlets open. Angle of attack of 0 degrees, freestream Mach number of 0.12, and engine face Mach number of 0.528.

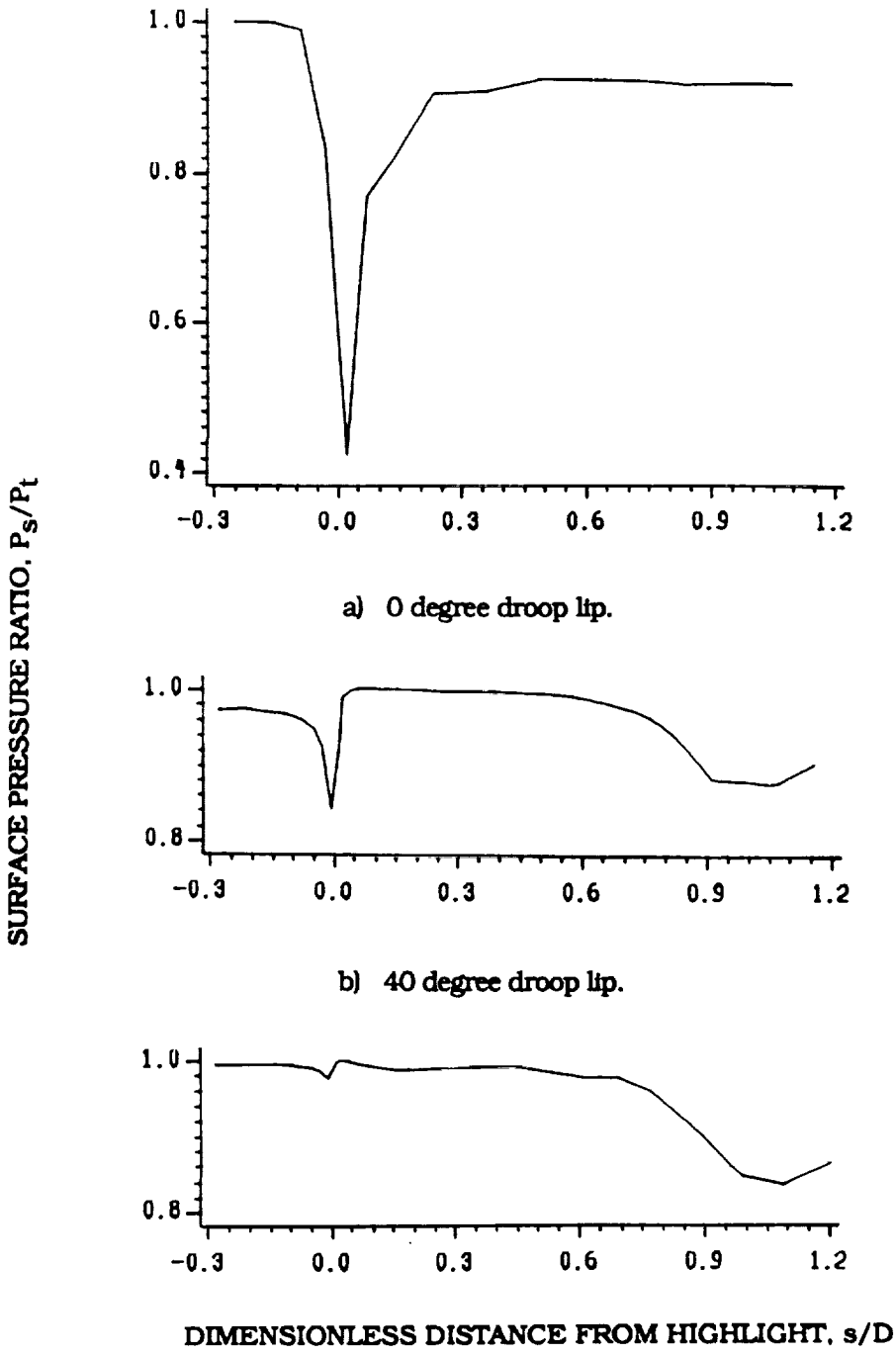

Figure 25. Comparison of surface pressure distribution for the 0, 40, and 70 degree droop cowl lip of the supersonic V/STOL inlet at a freestream Mach number of 0.12, control station Mach of 0.45, and an angle of attack of 30 degrees.

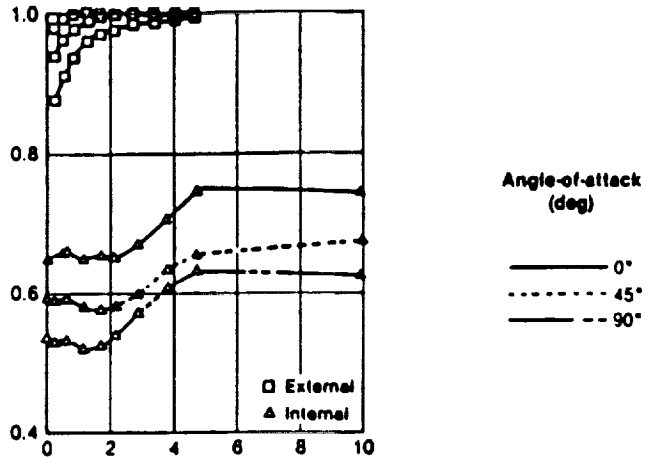

a) Sharp cowl lip; Effect of angle of attack.

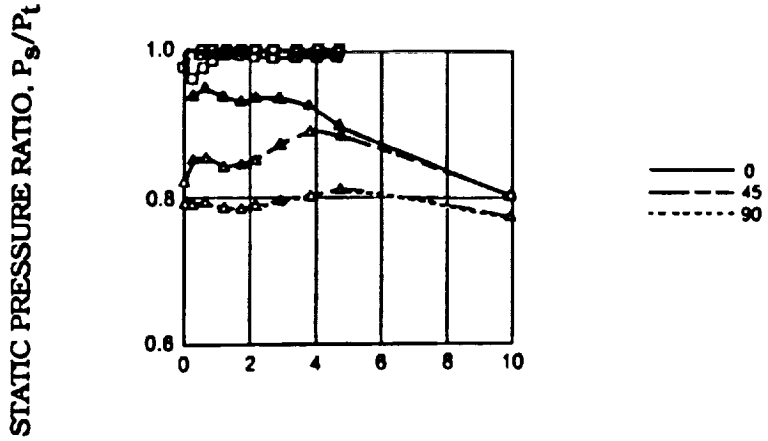

b) 40 degree droop lip; Effect of angle of attack.

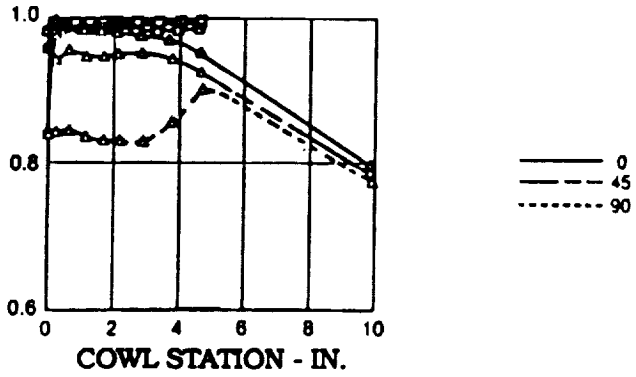

c) 70 degree droop lip; Effect of angle of attack.

Figure 26. Wind tunnel results of 0, 40, and 70 degree droop lip for angles of attack of 0, 45, and 90 degrees (Ref. 16).

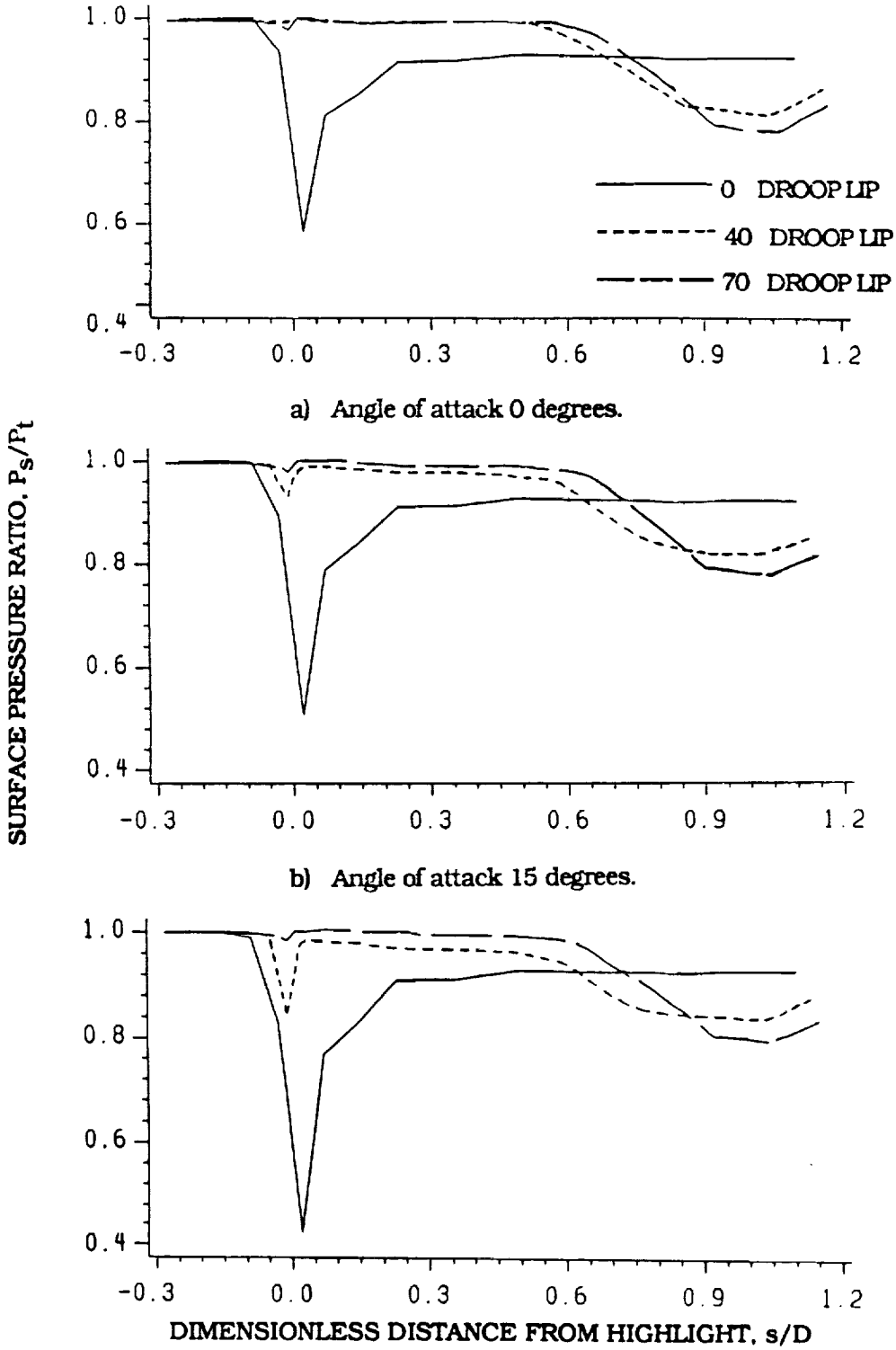

a) Angle of attack 0 degrees.

b) Angle of attack 15 degrees.

c) Angle of attack 30 degrees.

Figure 27. Calculated surface pressure distribution for the 0, 40, and 70 degree droop cowl lip of the supersonic V/STOL inlet at a freestream Mach number of 0.12 and control station Mach number of 0.45.

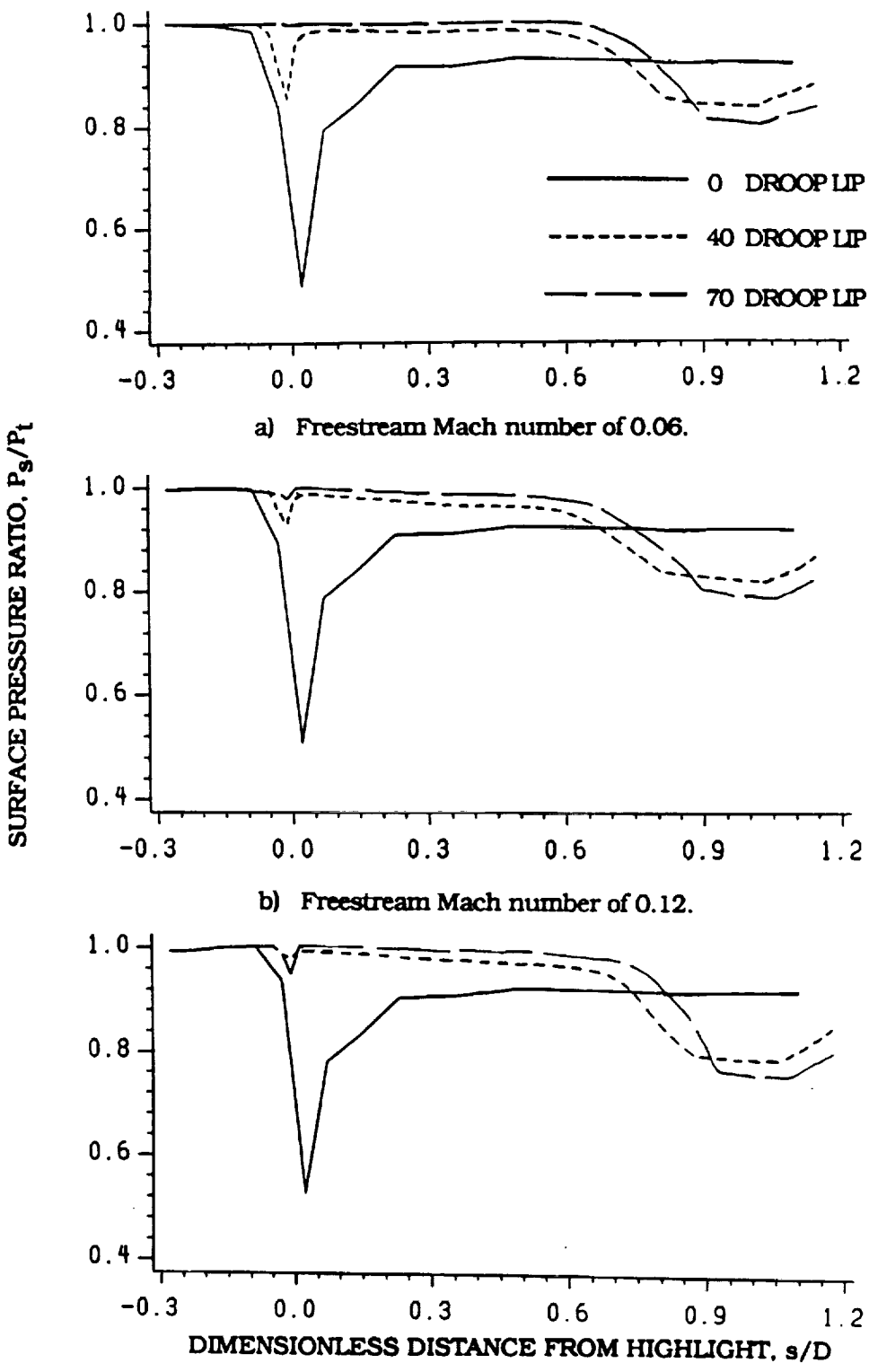

a) Freestream Mach number of 0.06.

b) Freestream Mach number of 0.12.

c) Freestream Mach number of .18.

Figure 28. Calculated surface pressure distribution for the 0, 40, and 70 degree droop lip of the supersonic V/STOL inlet at a control station Mach number of 0.45 and a angle of attack of 15 degrees.

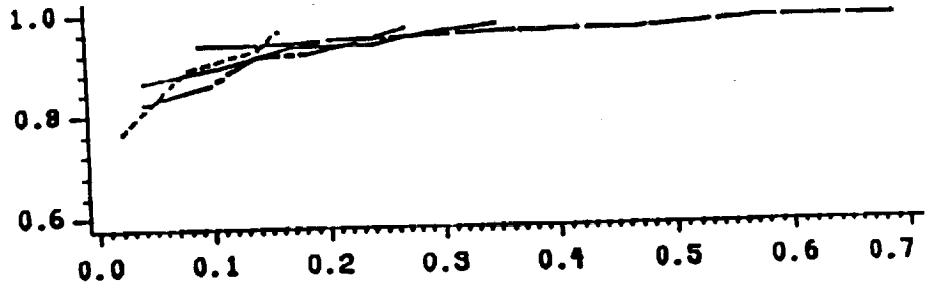

a) Forward Ramp.

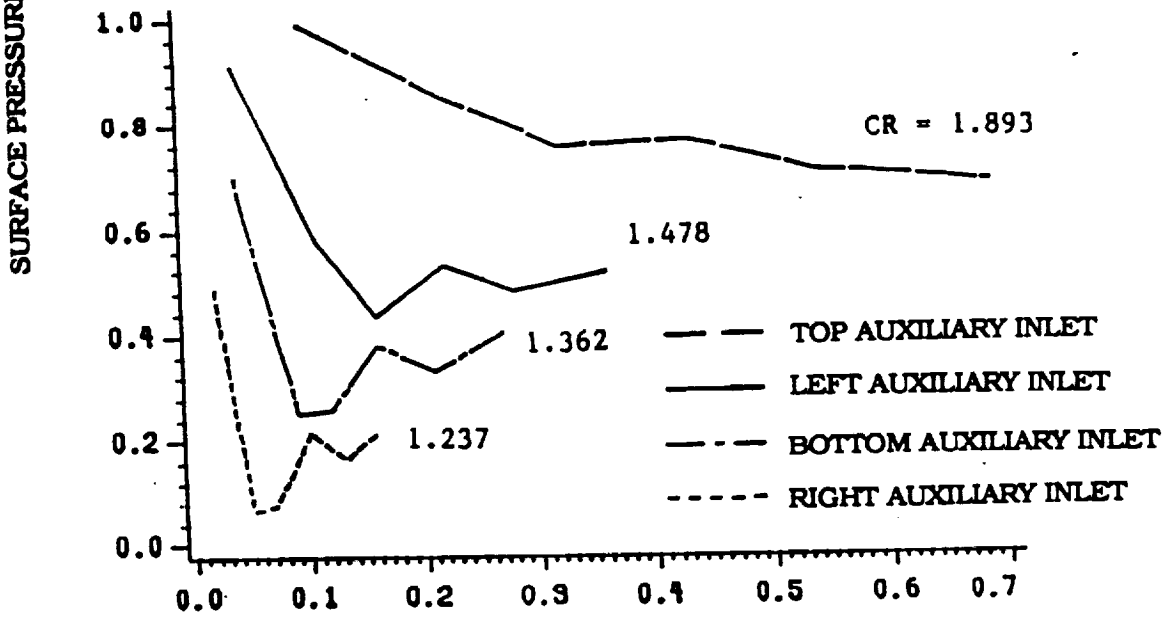

b) Aft Ramp.

Figure 29. Comparison of surface pressure distribution for the top, left, bottom, and right auxiliary inlets at a freestream Mach number of 0.12 and control station Mach number of 0.45.

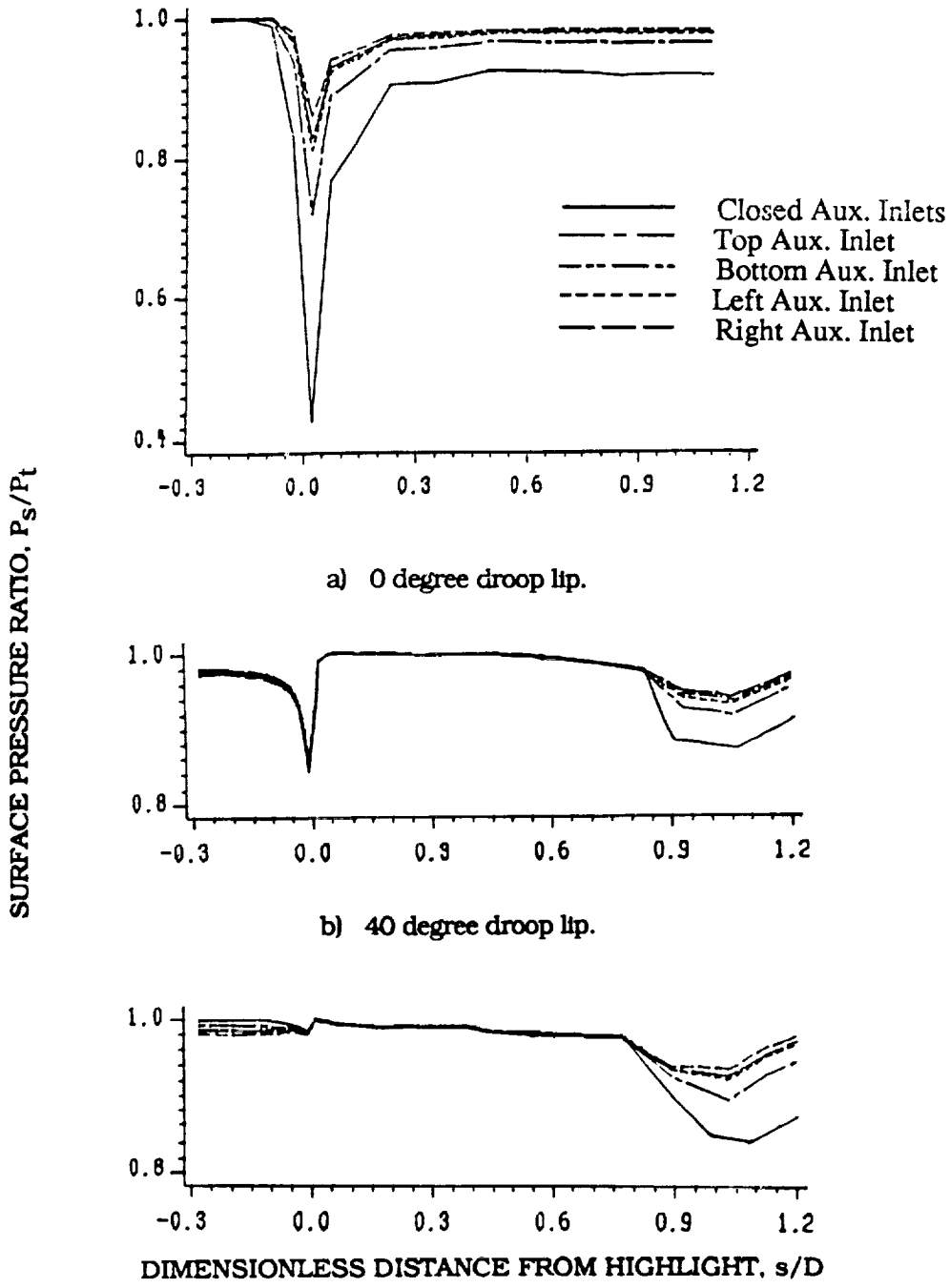

Figure 30. Effect of auxiliary inlets on surface pressure distribution for the 0, 40, and 70 degree droop cowl lip of the supersonic V/STOL inlet at a freestream Mach number of 0.12, control station Mach number of 0.45, and an angle of attack of 30 degrees.

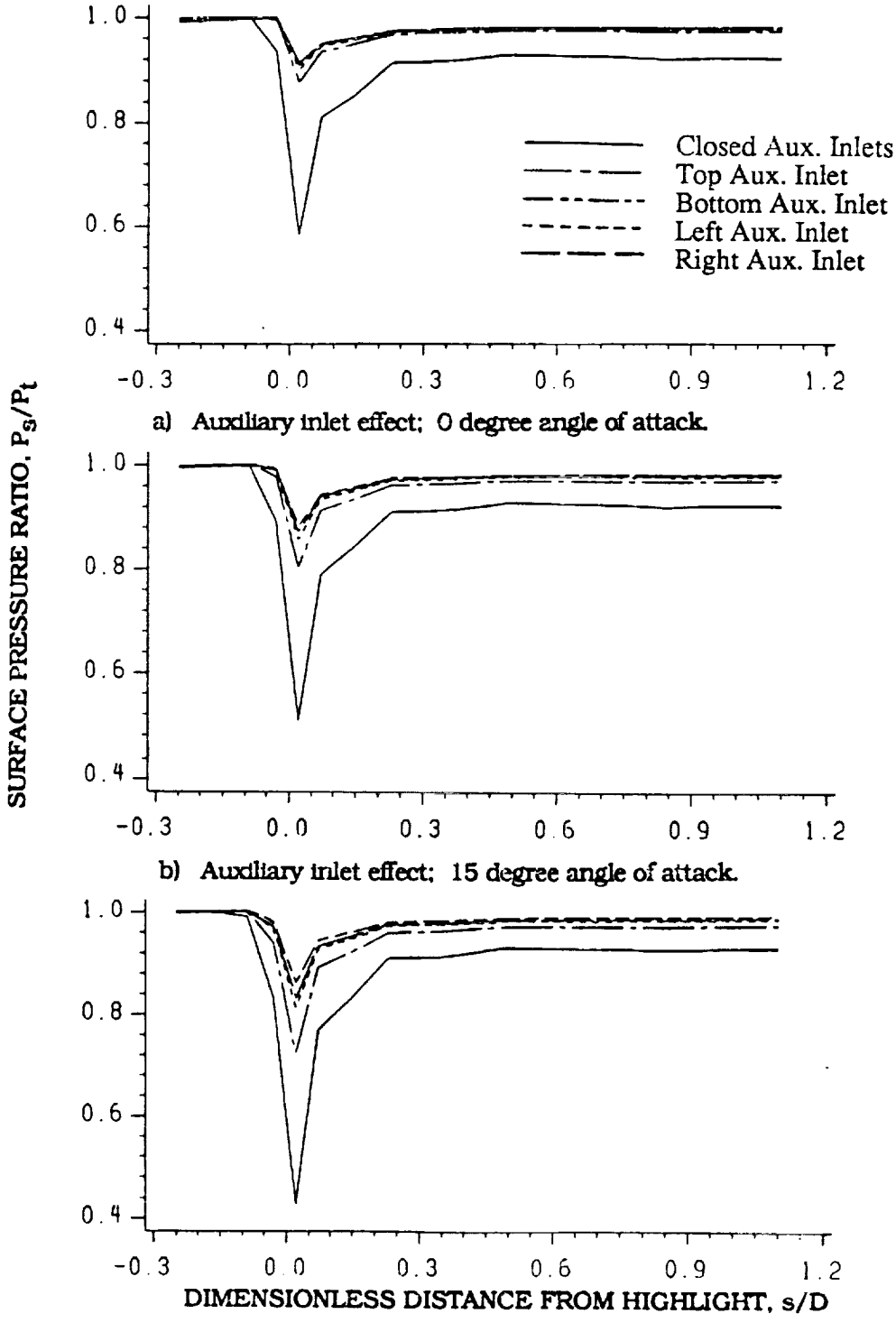

a) Auxiliary inlet effect; 0 degree angle of attack.

b) Auxiliary inlet effect; 15 degree angle of attack.

c) Auxiliary inlet effect; 30 degree angle of attack.

Figure 31. Effect of auxiliary inlets on surface pressure distribution for 0 degree cowl lip of the supersonic V/STOL inlet at a freestream Mach number of 0.12 and control station Mach number of 0.45.

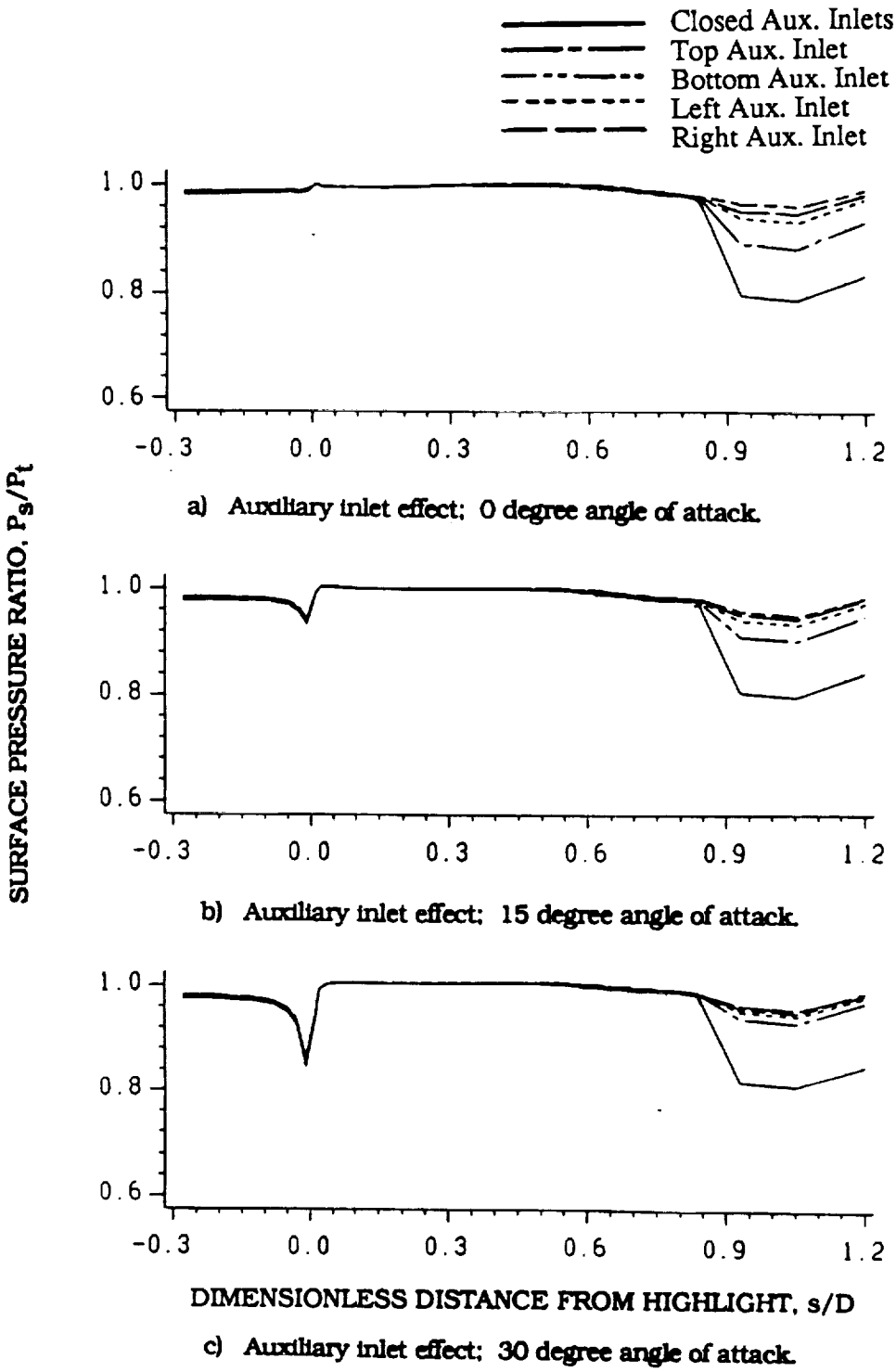

Figure 32. Effect of auxiliary inlets on surface pressure distribution for 40 degree cowl lip of the supersonic V/STOL inlet at a freestream Mach number of 0.12 and control station Mach number of 0.45.

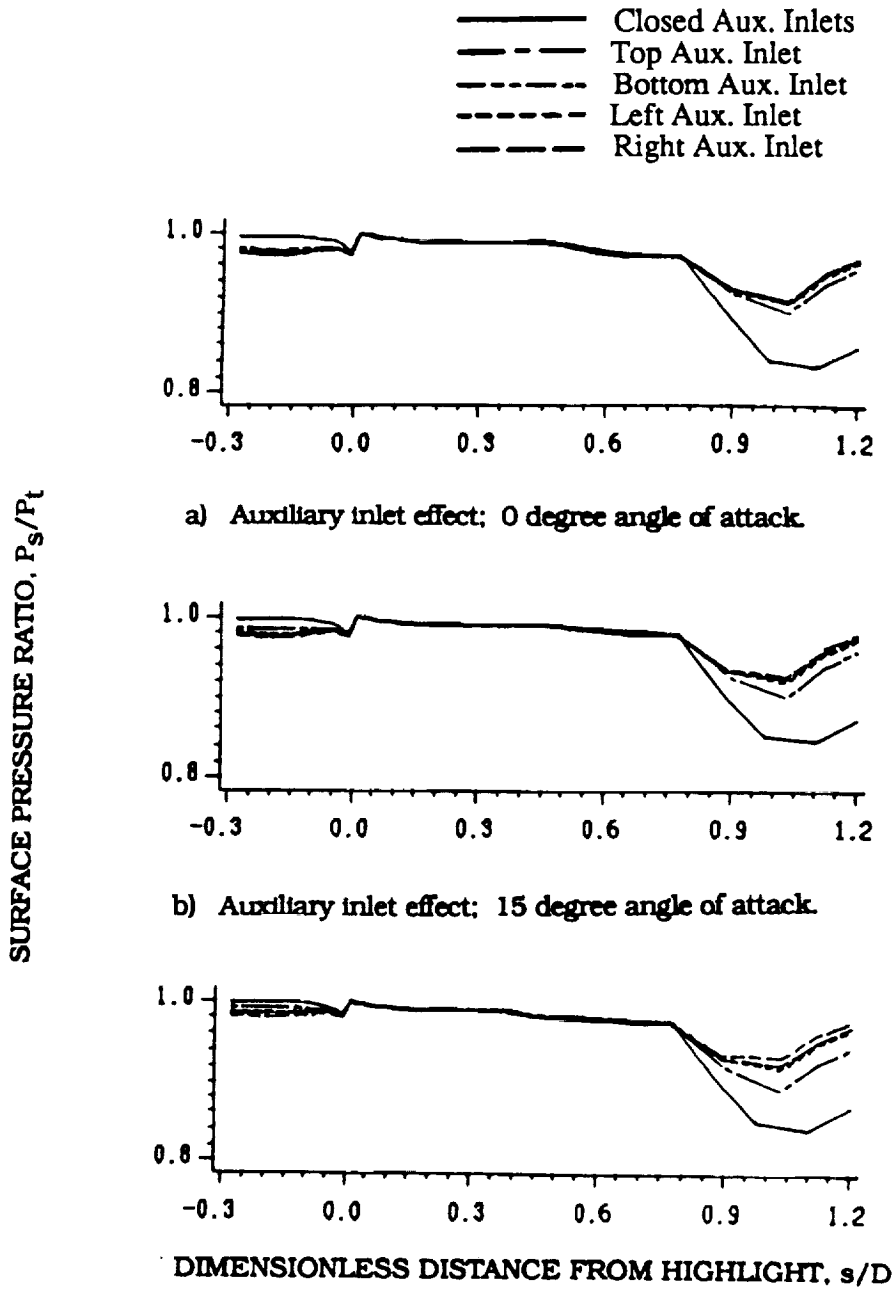

Figure 33. Effect of auxiliary inlets on surface pressure distribution for 70 degree cowl lip of the supersonic V/STOL inlet at a freestream Mach number of 0.12 and control station Mach number of 0.45.

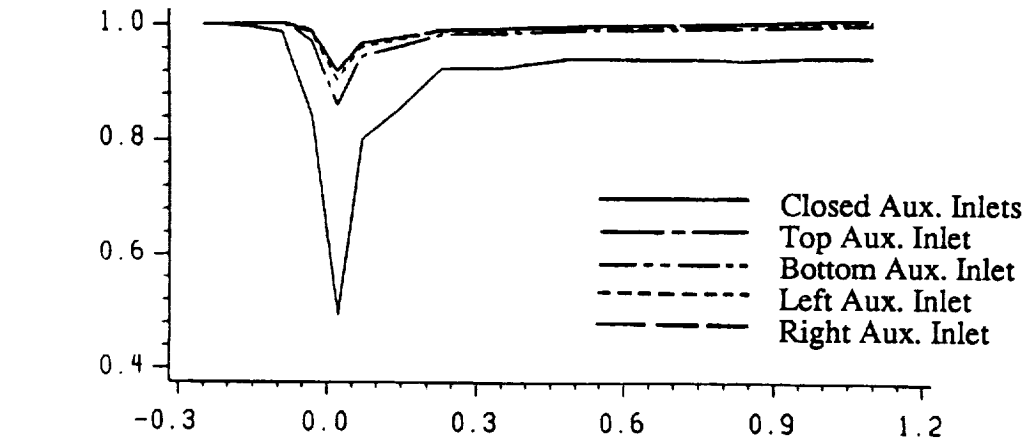

a) Auxiliary inlet effect; 0.06 freestream Mach number.

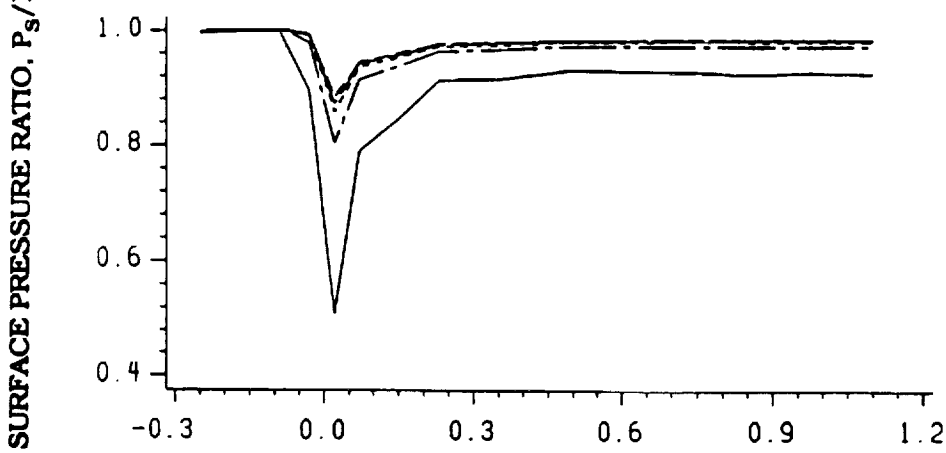

b) Auxiliary inlet effect; 0.12 freestream Mach number.

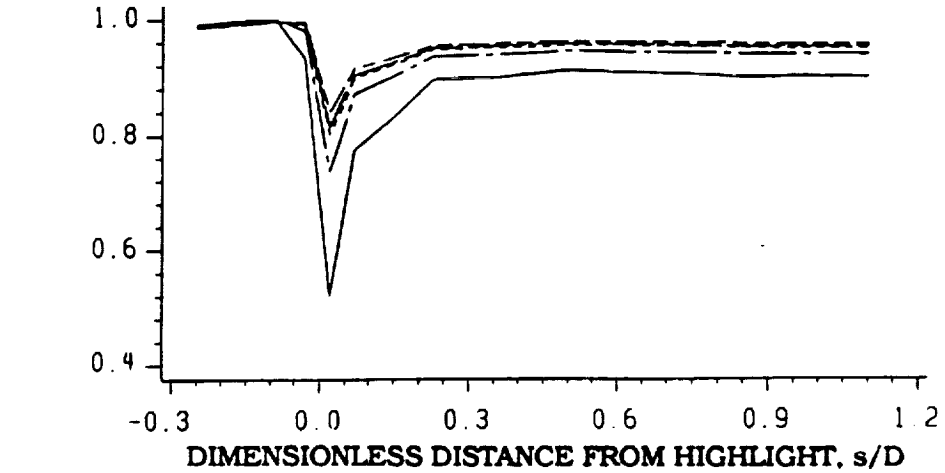

c) Auxiliary inlet effect; 0.18 freestream Mach number.

Figure 34. Effect of auxiliary inlets on surface pressure distribution for the 0 degree cowl lip of the supersonic V/STOL inlet at a control station Mach number of 0.45 and a angle of attack of 15 degrees for freestream Mach numbers of 0.06, 0.12, and 0.18.

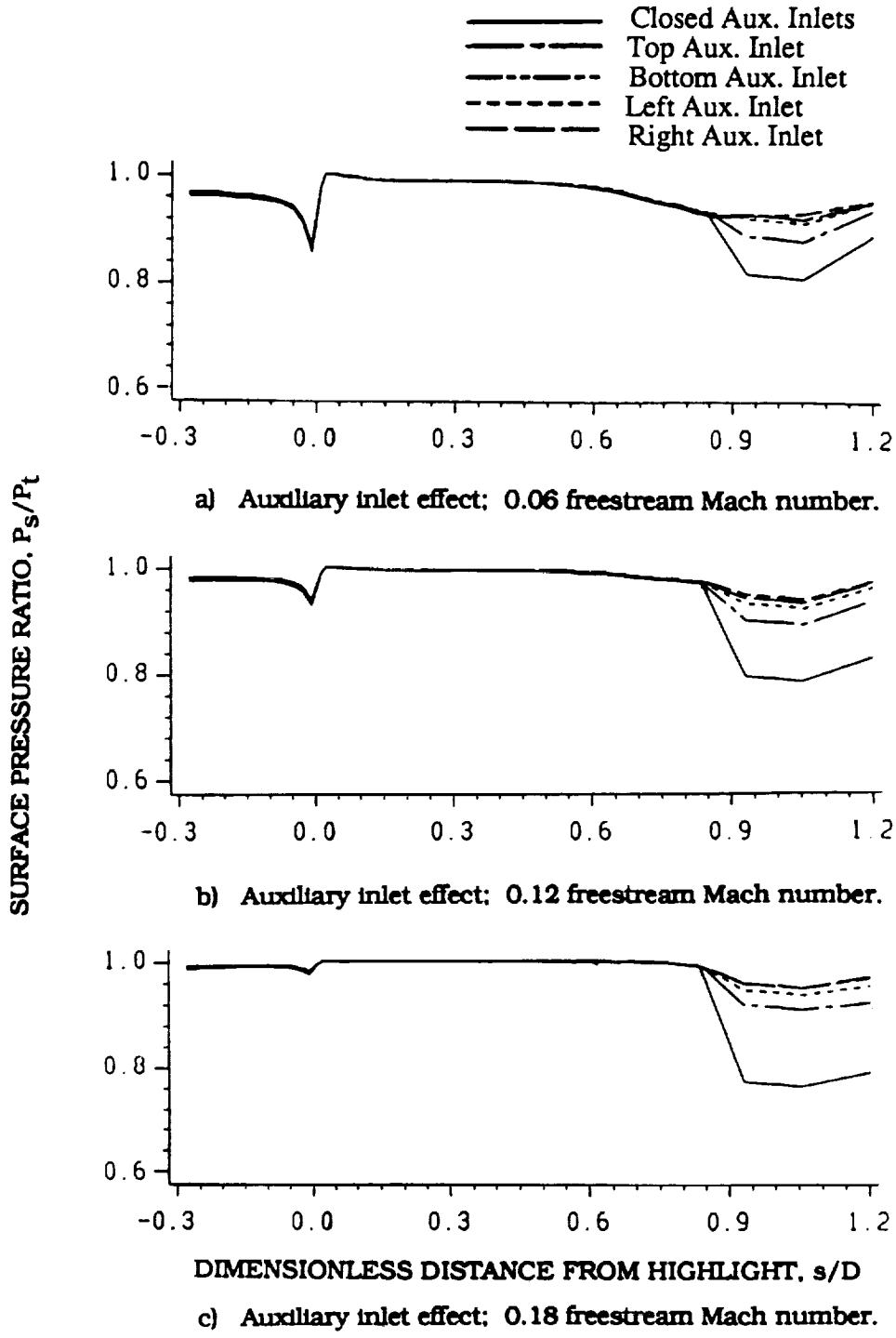

Figure 35. Effect of auxiliary inlets on surface pressure distribution for the 40 degree cowl lip of the supersonic V/STOL inlet at a control station Mach number of 0.45 and a angle of attack of 15 degrees for freestream Mach numbers of 0.06, 0.12, and 0.18.

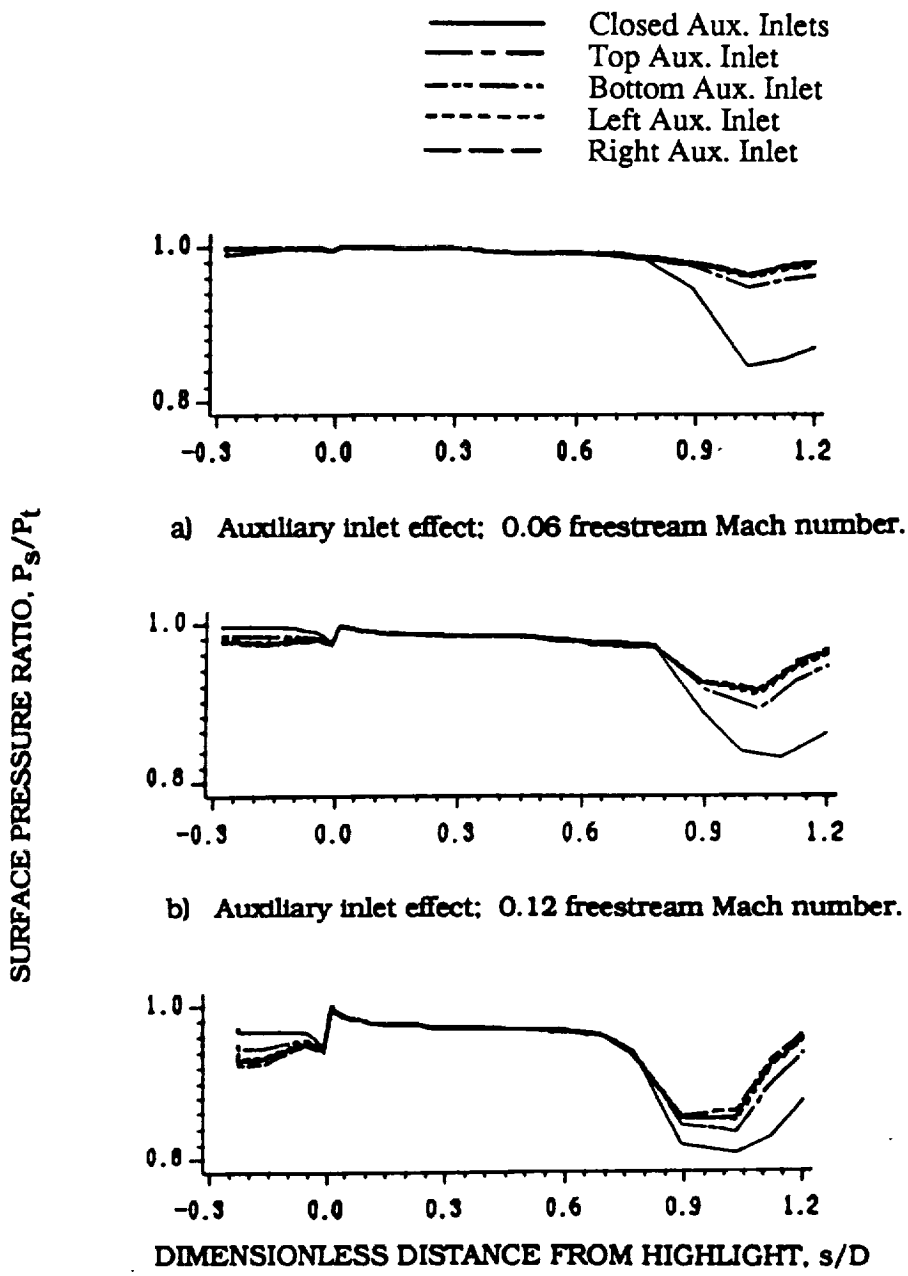

a) Auxiliary inlet effect: 0.06 freestream Mach number.

b) Auxiliary inlet effect: 0.12 freestream Mach number.

c) Auxiliary inlet effect: 0.18 freestream Mach number.

Figure 36. Effect of auxiliary inlets on surface pressure distribution for the 70 degree cowl lip of the supersonic V/STOL inlet at a control station Mach number of 0.45 and a angle of attack of 15 degrees for freestream Mach numbers of 0.06, 0.12, and 0.18.

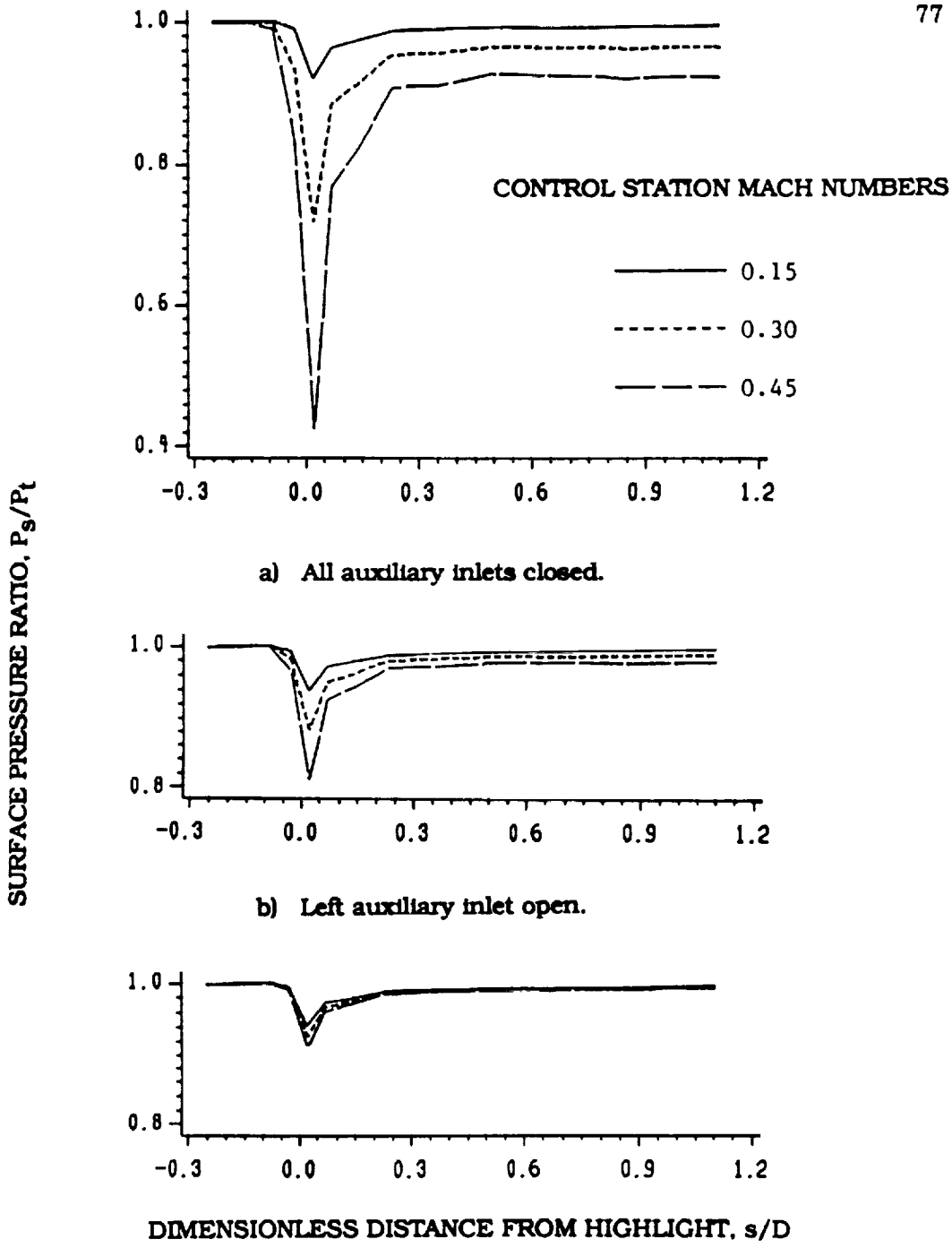

Figure 37. Comparison of surface pressure distribution for the 0 degree cowl lip of the supersonic V/STOL inlet at control station Mach numbers of 0.15, 0.30, and 0.45 at a freestream Mach number of 0.12.

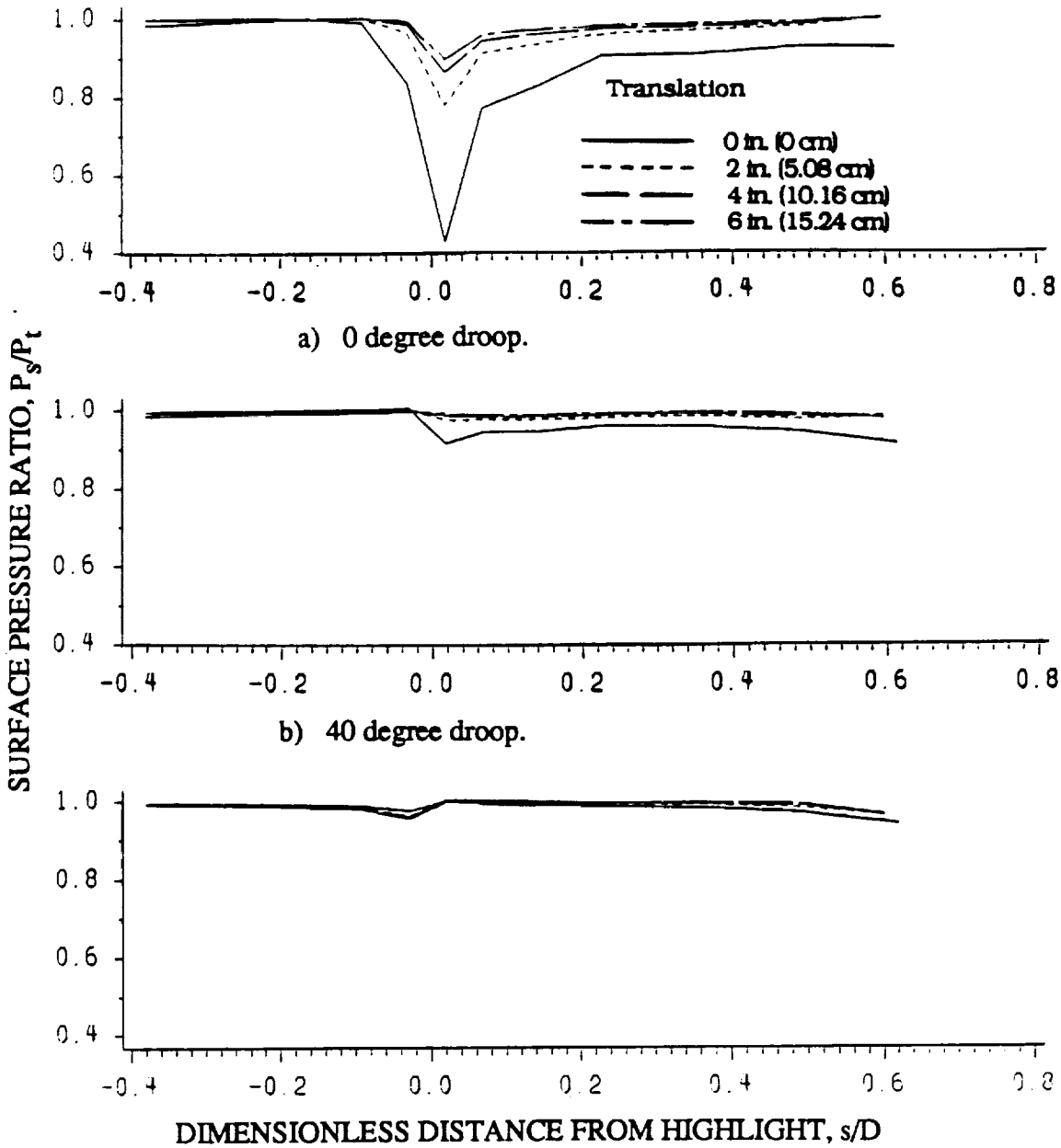

a) 0 degree droop.

b) 40 degree droop.

c) 70 degree droop.

Figure 38. Effect of lower lip translation on surface pressure distribution for the 0, 40, and 70 degree droop cowl lip of the supersonic V/STOL inlet at a freestream Mach number of 0.12, control station Mach number of 0.45, and a 30 degree angle of attack.

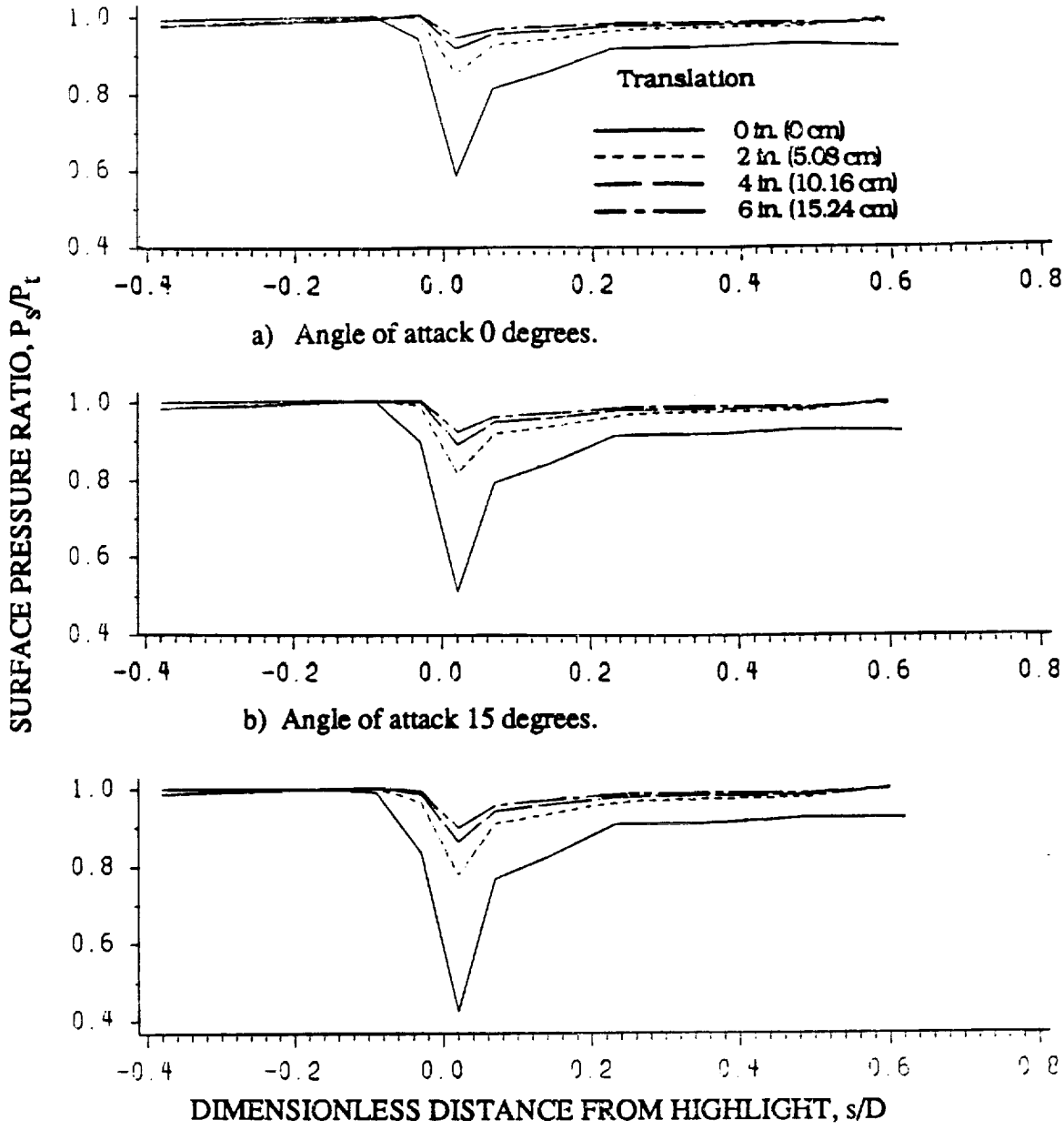

a) Angle of attack 0 degrees.

b) Angle of attack 15 degrees.

c) Angle of attack 30 degrees.

Figure 39. Effect of lower cowl lip translation on surface pressure distribution for 0, 15, and 30 degree angles of attack of the supersonic V/STOL inlet at a freestream Mach number of 0.12, control station Mach number of 0.45, and a 0 degree droop cowl lip.

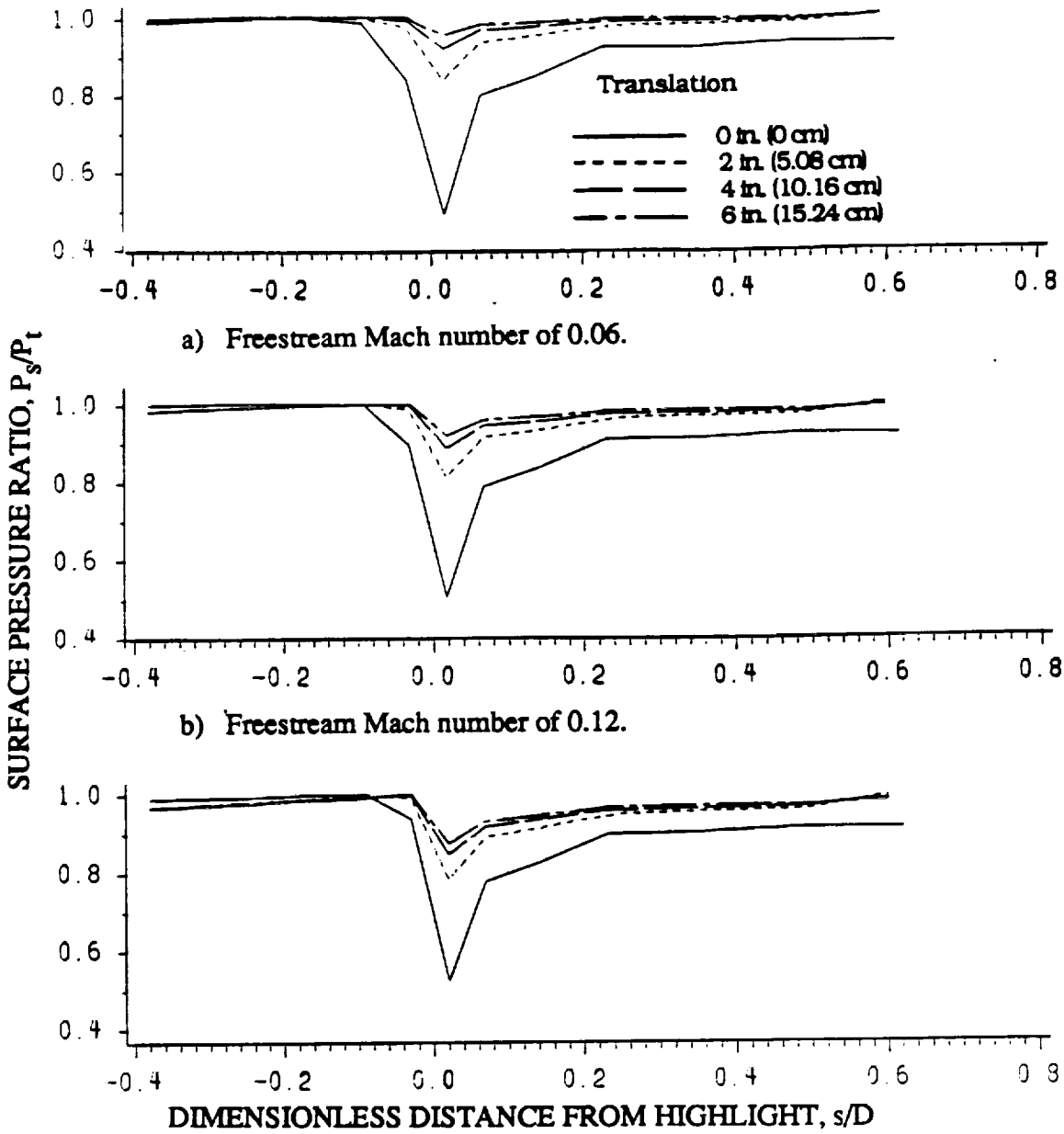

a) Freestream Mach number of 0.06.

b) Freestream Mach number of 0.12.

c) Freestream Mach number of 0.18.

Figure 40. Effect of lower cowl lip translation on surface pressure distribution for 0.06, 0.12, and 0.18 freestream Mach numbers of the supersonic V/STOL inlet at a control station Mach number of 0.45, 15 degree angle of attack, and a 0 degree droop cowl lip.

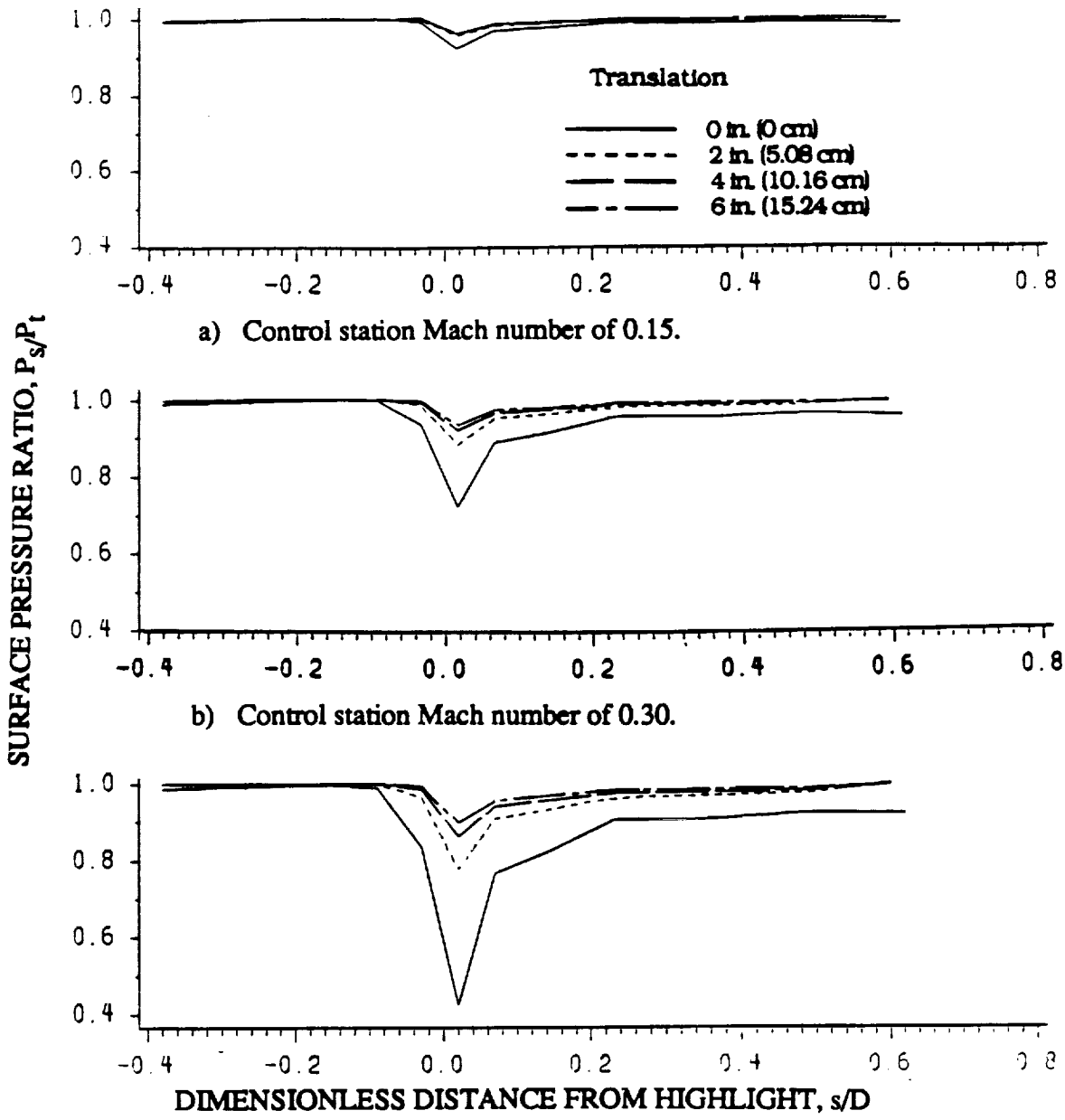

a) Control station Mach number of 0.15.

b) Control station Mach number of 0.30.

c) Control station Mach number of 0.45.

Figure 41. Effect of lower cowl lip translation on surface pressure distribution for 0.15, 0.30, and 0.45 control station Mach numbers of the supersonic V/STOL inlet at a freestream Mach number of 0.12, 30 degree angle of attack, and a 0 degree cowl lip.

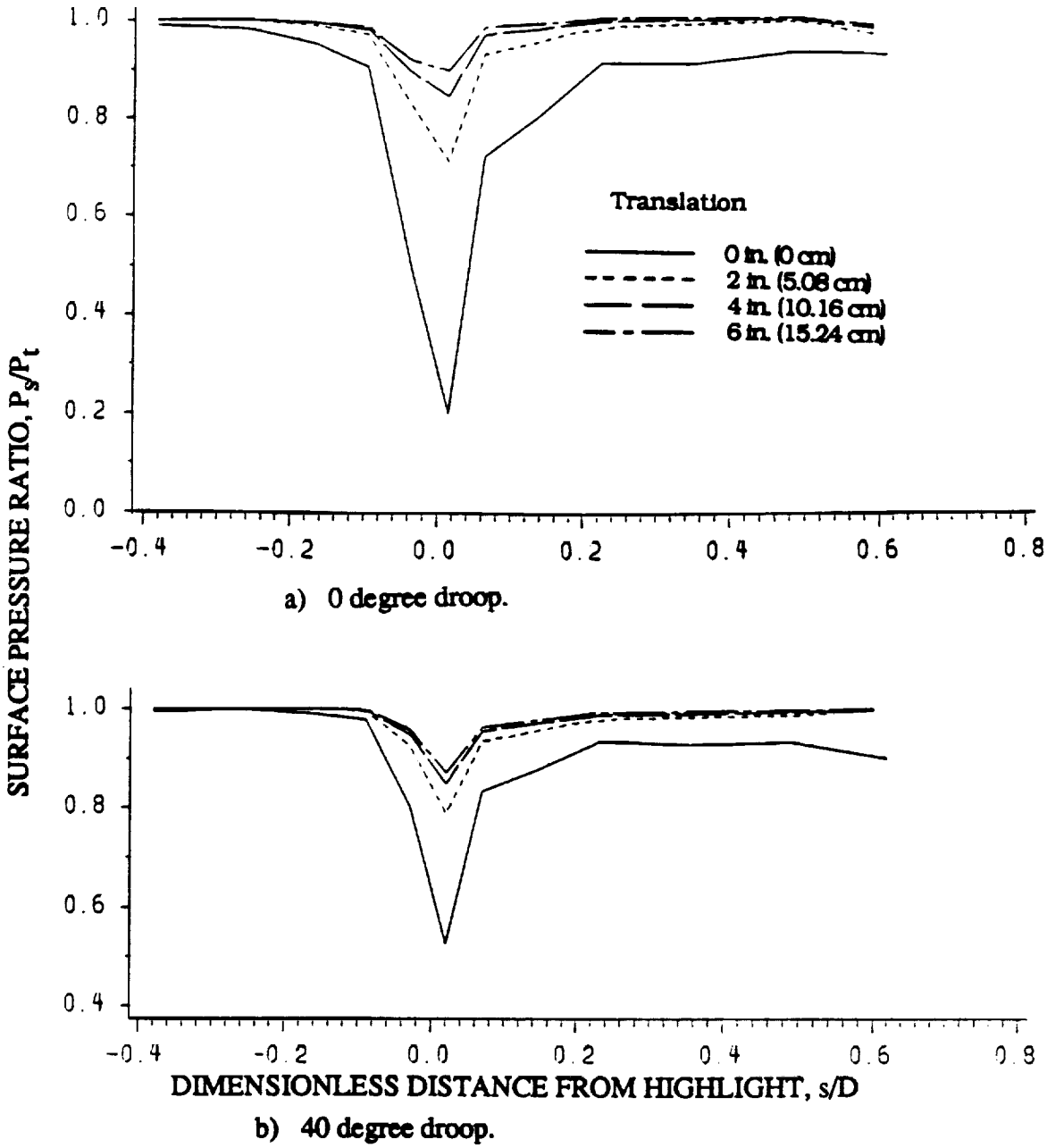

Figure 42. Effect of lip translation on surface pressure distribution for 0 and 40 degree droop cowl lips of the supersonic V/STOL inlet at a 90 degree angle of attack, 0.12 freestream Mach number, and 0.45 control station Mach number.

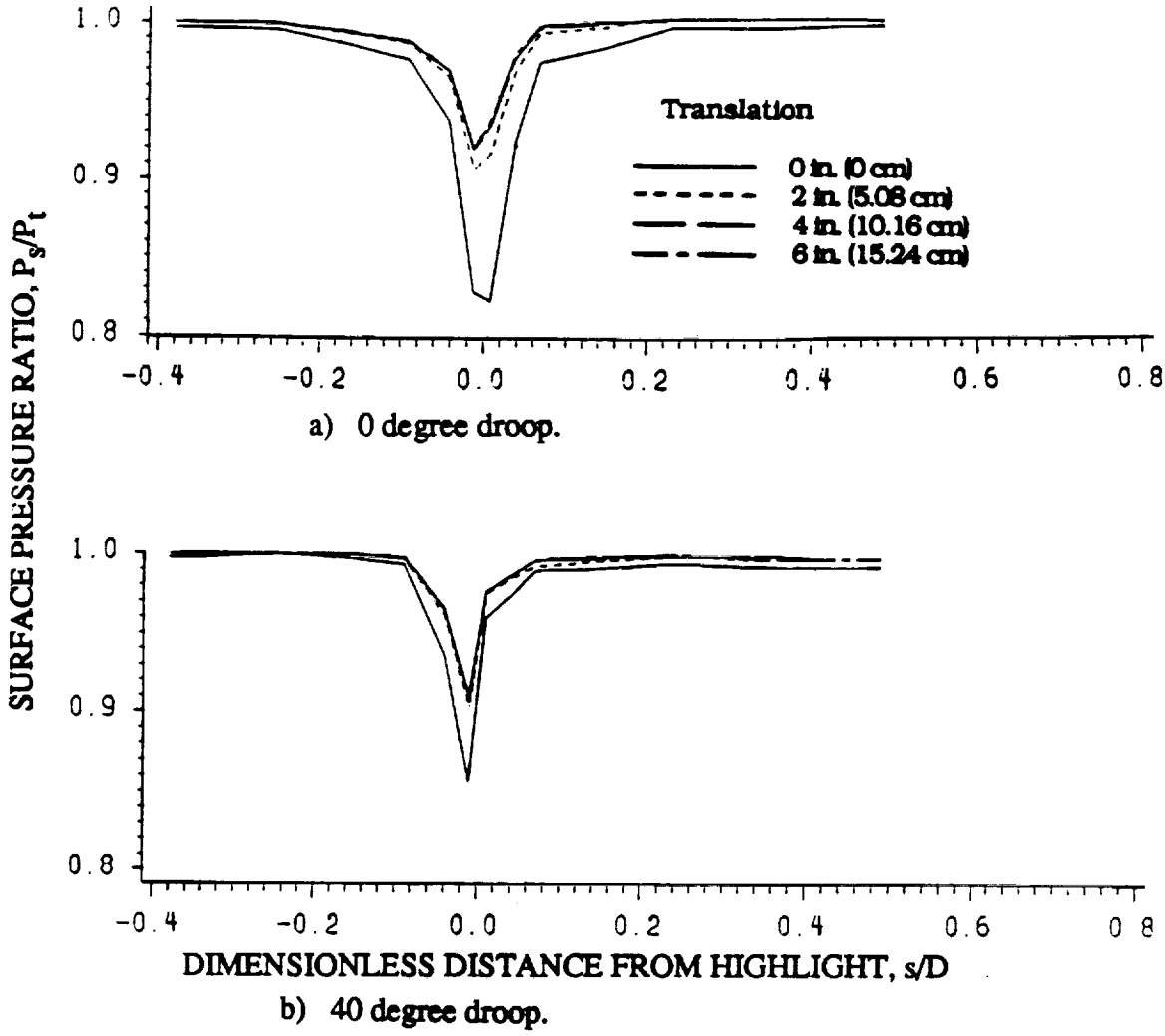

Figure 43. Effect of lip translation on surface pressure distribution for 0 and 40 degree droop cowl lips, with bottom port included, of the supersonic V/STOL inlet at a 90 degree angle of attack, 0.12 freestream Mach number, and 0.45 control station Mach number.

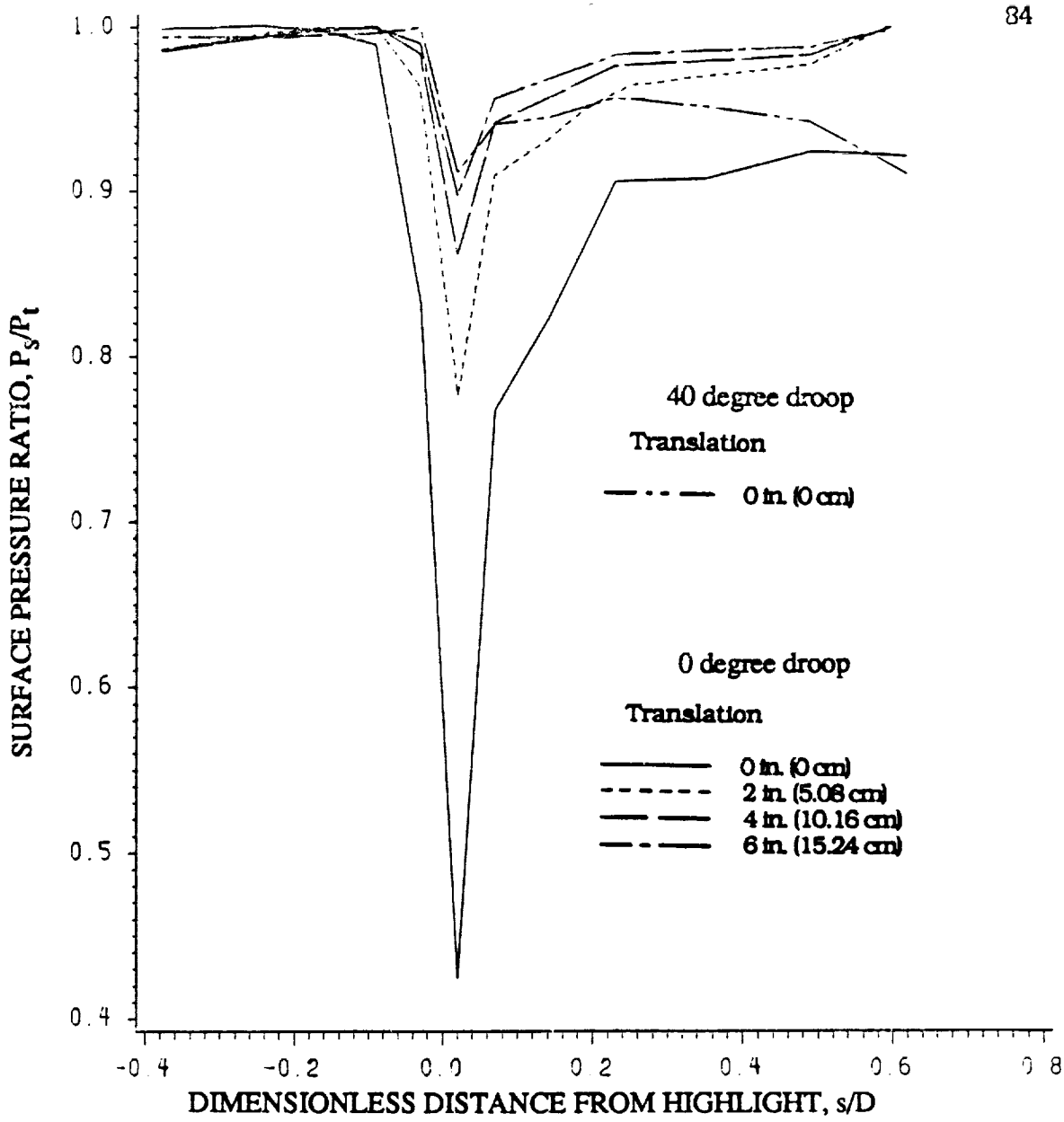

Figure 44. Comparison of surface pressure distribution for a 0 degree droop inlet at 0, 2, 4, and 6 in. (0, 5.08, 10.16, and 15.24 cm) translations and a 40 degree droop inlet at 0 in. (0 cm) translation of the supersonic V/STOL inlet at 0.12 freestream Mach number, 0.45 control station Mach number, and 30 degrees angle of attack.

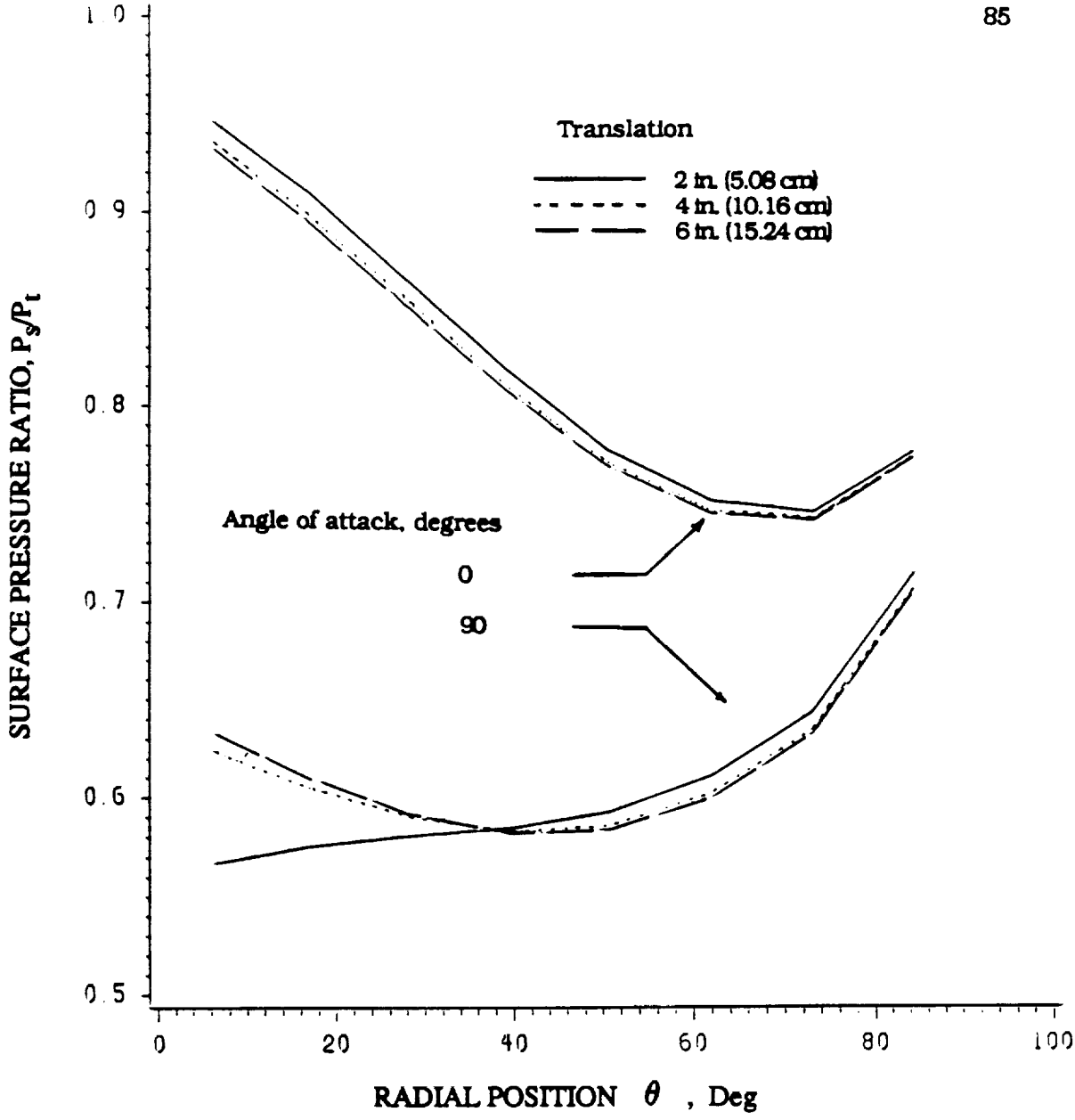

Figure 45. Aft-Ramp surface pressure distribution for 2, 4, and 6 in. (5.08, 10.16, and 15.24 cm) translations at 0 and 90 degree angles of attack, 0.12 freestream Mach number, and 40 degree droop cowl lip.

C2